Studies on the solid-state transformation and chemical modification reactions of carbon black nanoparticles

Vijayshankar Asokan

Dissertation for the degree of philosophiae doctor (PhD)
at the University of Bergen

2015

Dissertation date: 26.06.2015

Dedicated to my brother

Perarivalan and Arputhammal

Acknowledgements

I express my sincere thanks to Dorte Nørgaard Madsen, Associate professor, Department of Physics and Technology, University of Bergen, Bergen, Norway. Without her supervision and experience, I would not be able to accomplish this task. She also had great confidence in me and supported me throughout the work. Since from the beginning of my career in University of Bergen, she provided me a complete freedom in all stages of research work which gave space for me to design the project and conduct it.

I specially thank my beloved friend Dr. Vishnukanthan Venkatachalapathy, Researcher, Centre for Materials science and Nanotechnology Physics, University of Oslo, Oslo, Norway, who supported me in setting up research framework for my doctoral activities and encouraged me throughout my research life in Norway.

I heartily thank Professor Pawel Kosinski, Department of Physics and Technology, University of Bergen, Bergen, Norway and Dr. Velaug Myrseth Oltedal, Researcher, SINTEF Petroleum AS, Bergen, Norway, for their constant support and discussions throughout my research period and for their effort and time in writing scientific papers together with me.

I am very grateful to Professor Dayalan Velauthapillai, University College of Bergen, Bergen, Norway, who extended his support to make all the successful steps to complete my project.

I sincerely thank Professor Geir Anton Johansen, former Head of the Department of Physics and Technology, University of Bergen, Bergen, Norway, who made constructive steps in support of my doctoral activities during the period 2011-2012.

I thank Rachid Maad, Lab Engineer, Department of Physics and Technology, University of Bergen, Norway, who worked together with me to setup nano lab, without him my experiments and characterization works might be hard.

I thank Dr. Klaus Magnus Johansen, Norwegian Micro- and Nano-Fabrication Facility, NorFab –University of Oslo, who supported me with short term grant to carry out part of my research works at University of Oslo. The Research Council of Norway is acknowledged for the support to the NorFab (197411/V30).

It is worth to mention the role of my beloved friends Dr. Navaneethan Muthusamy (now at NTNU, Norway), and Boobalan Kasilingam (now at VIT, Vellore, India), for their help in the characterization and analysis part.

I thank my father Mr. Asokan, periamma Ms. Punithavathi, and my wife Ms. Elavarasi Valentina Deenadayalan. Their relationship made my life enthusiastic which make me to take constructive decisions in my research period. I would also like to thank my friends Dr. Sivakanesan and Sri Balasundaram who continuously encouraged and supported me in my personal life in Bergen.

Abstract

Carbon black (CB) is nanoscale particles with quasi-spherical nature, produced from incomplete combustion of hydrocarbons. It is a well-known type of amorphous carbon which exists in the form of aggregated spheres. CBs are most versatile materials, as the surface and structure can be easily tuned and/or modified, to target specific applications. The modification is generally straightforward in carbon materials both in nano and microscopic forms and it can either be done at the surface via chemical functionalization and/ or as structural transformation, where one form of carbon converts to another form either via catalytic or via non-catalytic processes.

CB belongs to the group of non-graphitizable carbon. The studies on the solid-phase transformation process of CB particles are carried out in the quest of obtaining further insight into the carbon nano structures.

In the present research work mono- and bi- metallic organic compounds were used as catalyst precursor and alumina boat as substrate to carry out solid- phase transformation studies. In the work, a straight forward, economical and single-step process for the transformation of CB nanoparticles into multi-walled carbon nanotubes (MWCNT), metal-encapsulated multi-walled carbon nanobeads (MWCNB) and nano-onion like carbon nanostructures is carried out.

Two CBs from different vendors (Timcal Graphite & Carbon and Cabot Corporation) having different surface areas and particle sizes, are used in these studies. The dependency of various effects (temperature, catalysts, catalyst to carbon ratio, substrate etc.,) on the degree of transformation and morphology of the resulting nanostructures are considered and studied widely in this project. The heating rate and catalyst to carbon weight ratio plays a crucial role in the determination of the success rate of the transformation process. Both these experimental parameters have been optimized to achieve a successful transformation of particles to tubes.

Comparison of the effect of platinum and iron as catalyst in this transformation process is also studied and discussed briefly on the basis of electron vacancies in d-

orbitals of metals. To our best knowledge, low temperature transformation study at 400° C is done and found to be successful in the formation of graphitized nanostructures.

Further, this works reported the transformation of CB using microwave energy with and without use of any metal catalysts and achieved in obtaining nano-balls, nano-onions and nano-sticks. Time of exposure to microwave irradiation is found to be crucial in the determination of morphology of the carbon products.

Electron microscopes (Scanning, transmission and high-resolution transmission), Raman spectroscopy, Thermal gravimetric analysis (TGA), X-ray diffraction (XRD) methods have been used for the characterization of the samples.

The second project deals with the chemical modification of CB surface with the intention to provide simple and effective reaction technique. Hence, di- and tri-carboxylic acids have been used to functionalize the carbon surface. In addition, it does not require prolonged heating, filtration and washing as it is required when using mineral acids. As both the maleic and citric acid varies with the concentration of hydroxyl and carboxyl molecules, surface reactions on the carbon is expected to be different. The effect of solvents (water/ ethylene glycol) and the effect of pre-heat treatment of carbon have been studied. Both Timcal 350G and XC72R CB samples have been used in the chemical modification experiments. This work further studied the processes and shown the results varies with the solvent used and pre-heat treatments on CB.

The modified samples were characterized by thermo-gravimetric analysis (TGA), surface area analyzer, X-ray diffraction (XRD), particle size and Zeta potential measurements, and Fourier transform infra-red spectroscopy (FTIR). It is found that several material properties, among these the thermal stability and surface area of the modified carbon black, are significantly altered relative to the parental carbon samples.

List of publications

1. **V. Asokan**, P. Kosinski, T. Skodvin, V. Myrseth, "Characterization of carbon black modified by maleic acid*", **Frontiers of materials science**, 2013, 7(3), 302-307.*

2. **V. Asokan**, D. Velauthapillai, R. Løvlie, D.N. Madsen, "Effect of substrate and catalyst on the transformation of carbon black into nanotubes*", **Journal of materials science: Materials in electronics**, 2013, 24, 3231- 3239.*

3. **V. Asokan**, D.N. Madsen, D. Velauthapillai, V. Myrseth, P. Kosinski, "Effect of temperature on the transformation of carbon black into nanotubes*", **Advanced materials research**, 2014, 875-877, 1565-1571.*

4. **V. Asokan**, D.N. Madsen, P. Kosinski, V. Myrseth, "Transformation of carbon black into carbon nano-beads and nanotubes: the effect of catalysts", ***New carbon materials***, *2015, 30(1), 19-29.*

5. **V. Asokan**, V. Myrseth, P. Kosinski, "Effect of Pt and Fe catalysts in the transformation of carbon black into carbon nanotubes", ***Journal of physics and chemistry of solids,*** 2015, 81, 106-115.

6. **V. Asokan**, V. Venkatachalapathy, D.N. Madsen, "Microwave irradiation on carbon black nanoparticles: Studies on the transformation into nano-sticks and nano-onion structures", ***To be submitted***.

Related publications not included in the thesis

7. P. Kosinski, R. Nyheim, **V. Asokan**, T. Skjold" "Explosion of carbon black and propane hybrid mixtures*"* ***Journal of loss prevention in the process industries***, *2013, 26, 45-51.*

8. E. P. Subramaniam, G. Rajesh, N. Muthukumarasamy, M. Thamibidurai, **V. Asokan**, D Velauthapillai, "Cu_2ZnSnS_4 thin films solar cells prepared by chemical bath deposition method", ***Indian journal of pure and applied physics***, *2014, 52, 620-624.*

9. M. Marikannan, **V. Asokan**, V. Venkatachalapathy, J. Mayandi, "Preparation and characterizations of SnO thin films towards photovoltaic applications", ***AIP Advances,*** 2015, 5, 027122 (1-8).

Contents

Chapter 1

Introduction

1.1 Significance of carbon and nanocarbon

Carbon exists in several allotropic forms, of which graphite, diamond and amorphous carbon are well known. Carbon forms basis for all organic compounds and carbon compounds form the foundation of all known life on our planet. Nearly 10 million carbon compounds exist in our world.

Carbon has played an important role in human life throughout the history. Graphite was the first known pure carbon and has been used for many applications since early iron-age [1, 2]. Graphite in pencil and soot in black ink were used for writing, drawing and painting applications since the middle Age. Charcoal and soot are the amorphous carbon which have been known and utilized for various applications even during 5000 BC. Diamond is the hardest naturally occurring material [3, 4] and thought to have been first discovered in India around 4000 BC. Diamond is useful in scientific and medical applications in addition to just being an ornament. William Bragg and Lawrence Bragg used diamond for the first ever structure determination using X-ray diffraction [5].

Carbon has been used in its elemental forms in industry as early as before Thomas Edison used it to make the filaments for the light bulbs. Graphite-based new carbon materials (carbon fibers, glass-like carbons, pyrolytic carbons) synthesized in the 20th century, found broad industrial applications.

In the last decades, a number of new nanocarbon structures have been synthesized and find their applications in a wide range of fields from clothes, electronics, and sports equipment to mechanical, medical and biological applications. Carbon nanotubes (CNTs), fullerenes, carbon nano-fibers, carbon nano-rods, nano-diamonds, carbon nano-cones, carbon nano-horns, as well as carbon black (CB) are some of the

forms of nano carbon materials. CB was the first nano carbon materials to find applications in our world. CB is used in Indian black inks way back in history.

Graphene is a recently synthesized structure. The noble prize winner of 2010, Andre Geim and his colleagues used an amazingly simple technique which involved rubbing a freshly cleaved graphite surface against another surface and finally succeeded in isolating individual sheets of graphene. Graphene is a one-atom thick planar sheet of sp^2-hybridized carbon atoms. The atoms are densely packed in a honeycomb crystal lattice. Graphene is the basic structural element of some carbon allotropes including graphite, CNTs and fullerene. The carbon-carbon bond length in graphene is about 0.142 nm as in graphite.

Graphene and CNTs are useful in nano electronic devices and nano field emitters due to their inherent and excellent electronic properties because of their nanoscale nature. Some of the main areas where nanotubes find their applications are: ultimate reinforcement fibers for composites, field emitters (individual nanotube field emitters, large area flat panel displays,); nano tools (tips for Scanning Tunneling, Atomic Force, Magnetic Resonance Force and Scanning Near-field Optical, Chemical/Biological Force Microscope tips, nano manipulators, nano tweezers).

Carbon materials, both at the nano and microscopic level, have their scientific and technological attention in many applications till date, due to their diversity of chemical, physical, structural and electronic properties [6, 7]. One of the main advantages in using carbon for various applications is that most of the properties of carbon materials can be adjusted and modified, depending upon the target applications [8]. The modification is straight forward in many carbon materials both in nano and microscopic forms and it can either be done at surface level via chemical functionalization and or as structural transformation where one form of carbon converts to another form either via catalytic or non-catalytic processes.

In the present research work, CB material is studied in modification reactions. Both chemical and structural transformation studies were performed. Due to nanoscale effects, CB particles usually appear in the form of aggregates. CB is semi-amorphous

and consists of many individual graphite layers that are only roughly parallel to one another and it shows a notably larger spacing between the layers compared to that of graphite [9, 10].

Compared to other nano materials, CB possesses high specific surface area and good electronic conductivity and has relatively high stability in both acidic and basic media, and possesses good electronic conductivity and high specific surface area. Because of these qualities, CB is frequently used as a catalyst support [11].

The CB surface can be easily modified by introducing functional groups. By functionalizing the surface of CB, one alters the surface properties, and the hydrophilic or hydrophobic character of the surface may change according to the chemical nature of the surface groups. In addition, grafted components may provide nucleation sites for deposition of highly dispersed metal particles yielding potential materials for fuel cell catalysts with increased activity [11-13].

In addition to the above mentioned possibilities of applications, carbon nanostructures with metal-encapsulation find applications in electronic and biological fields [14]. The present works aims at synthesizing metal-encapsulated and graphitized carbon nanostructures in a simple and single heating process. Further, the studies on the solid-phase transformation process of CB particles are carried out in the quest of obtaining further insight into the carbon structures. In the current research, the transformation of CB was carried out at relatively low temperature compared to the work reported in references [15-17] and in a simple approach using a single stage furnace.

1.2 Thesis motivation and objectives

The motivation to this thesis project arises from the importance of CNT in the modern world and the studies on the transformation of CB to get insight into the carbon nano structures and secondly, the need for the surface functionalization of CB to improve its properties. Hence this thesis is structured into two projects, i) structural

modification of CB into CNT and ii) chemical modifications of CB using organic acids. However, majority of the work of the present project is devoted to the catalytic solid-phase transformation of CB into graphitized nanostructures and only a minor part focus on chemical modifications of CB.

Likewise, the objectives of the work split up into two part. In the first part of the project, the solid-phase transformation studies on the amorphous carbon nanoparticles (CB) into graphitized nanostructures (nanotubes, nano-beads, nano-onions, nano-balls, nano-sticks) have been carried out. Studies further aim at:

i) synthesizing good quality nanotubes with magnetic metal at the tip or encapsulated, by CVD methods with an effective and easy process,
ii) catalyst, substrate, carbon source and temperature are altered and the effects caused by such changes are studied to explore in depth phenomena in the catalytic transformation process of CB into graphitized nanostructures,
iii) optical and structural properties of synthesized products are studied and hence the material natures of as-synthesized products are evaluated.

Transition-metals like Fe, Ni or Co encapsulated in carbon nanostructures are magnetic and find potential applications in areas like medical treatments [18] and data storage [19]. Thus, we also carry out thermo-magnetic studies on few synthesized nanostructures to assess the temperature effect on the metal nanoparticles in carbon nanostructures as these nanostructures can be used in high temperature electronic and magnetic applications.

For the studies on the solid-phase transformation behavior of CB nanoparticles into different nanostructured products, three different experimental set ups were used: 1) thermal evaporation using ceramic boat and stainless steel as the substrate, 2) transformation using microwave irradiation and 3) transformation using CVD and a closed quartz tube. The CB used in these experiments was Ensaco 350G provided by Timcal Graphite & Carbon and Vulcan XC72R provided by Cabot Corporation hereafter referred as Timcal 350G and XC72R.

The second part of the project focuses on studying surface functionalization of CB. The chemical reactions using acids (mineral/organic acids) usually bring two modifications to the parental carbon: i) it will create carboxyl and/or hydroxyl surface functional groups and ii) morphological and textural changes.

In the present work, di- carboxylic and tri- carboxylic acids have been used for the surface functionalization reactions of CB. The effect of solvents (water/ ethylene glycol) and the effect of pre-heat treatment of carbon have been studied. Both Timcal 350G and XC72R CB samples have been used in the chemical modification experiments.

The structure of the thesis is as follows: In chapter 2, a basic introduction about CB and its structure and properties are discussed, brief introduction to graphite, graphene and nanotubes have also been given. Introduction to the solid-phase transformation of amorphous carbon nanoparticles into graphitized nanostructures and an introduction to chemical modifications of CB are given in chapter 3. In chapter 4, the characterization methods, which are used to study the properties of CB, modified CB and nanotubes are described. Results and discussion about the effect of catalysts, substrates, temperature, carbon to catalyst ratio and the effect of microwave irradiation in the structural transformation of CB are discussed in chapter 5. Studies on chemical modifications of commercially available CBs are also included in chapter 5. Finally, chapter 6 summarizes the whole project and ends the thesis with conclusion and suggestion for the future works.

Chapter 2

Introduction to Carbon nanostructures

2.1 Carbon and its allotropes

Carbon is usually described by the symbol C, its atomic number 6 and holds an electronic configuration of $1s^2$, $2s^2$, $2p^2$ [20]. Out of these three atomic orbitals, $1s^2$ contains two strongly bound core electrons. The valence $2s^2$, $2p^2$ orbitals are occupied by four weekly bound electrons. Carbon materials are distinct due to its nature of hybridization of the atomic orbitals. Because of many possible configurations of the electronic states of a carbon atom and its relation to the bonding of two nearest carbon atoms, carbon forms many allotropes with different physical and structural properties.

Allotropes of carbon include diamond, graphite, amorphous carbon, fullerenes and nanotubes. Diamond is well known for its extreme hardness because of its sp^3 hybridized carbon atoms and in turn forms strong covalent bonding between nearest carbon atoms. Graphite consists of layered and planar structure with pure sp^2 hybridized carbon atoms within an each layer. It is soft in nature with attractive properties. Amorphous carbon includes soot and CB does not have any crystalline properties, available in nanoscale. Fullerene and CNTs are also at nanoscale carbon materials.

In this chapter, particular emphasize has been given to amorphous carbon, graphite and nanotubes.

2.2. Carbon Black– an introduction

Carbon black (CB) is nanoscale particles with quasi-spherical nature and form of an amorphous carbon, produced from incomplete combustion of hydrocarbons [21]. The size of CB particles vary from 10 to 1000nm depending on the production processes

[21, 22]. CB contains more than 90% carbon as well as hydrogen and oxygen. Usually, the CB surface has chemisorbed oxygen complexes (such as carboxylic, quinonic, lactonic, phenolic groups and others) to varying degrees, but the ratio depends on the manufacturing process [21]. CB was used as a pigment in black ink used by Chinese and Indians in third century B.C.

CB manufacturing process is essentially classified into two major categories, incomplete combustion and thermal decomposition, depending upon the presence or absence of oxygen. Thermal decomposition process plays only a limited role while incomplete combustion process is more important and plays vital role in terms of producing major quantities.

In-complete combustion is also termed as thermal oxidative decomposition can be further classified with respect to the flow criteria, turbulent flow and diffusion flames. In turbulent flow system, the production process can be divided into furnace black process, lamp black process and in diffusion flames system, the production process is called as channel black process. Thermal decomposition process is further classified into thermal black process and acetylene black process.

Both the projects discussed in this thesis used commercial carbon blacks, Vulcan - XC72R from Cabot Corporation, Ensaco 350G from TIMCAL Graphite and Carbon.

2.2.1. Physical properties of CB

Due to nanometer-size effects, CB particles usually appear in the form of aggregates. CB is semi-amorphous and consists of many individual graphite layers arranged roughly parallel to one another but in random orientation about the normal to the layer and shows notably larger in spacing between the layers compared to that of graphite [9, 10]. Although CB does not have the three-dimensional repetition of graphite, there are finite two-dimensional repetition within each layer and hence CB is termed as ‘turbostratic’ as its structure is between amorphous and graphitic [23]. In other words, Hexagonal graphite (h-graphite) has an ABAB stacking structure

while graphene layers in turbostratic graphite (t-graphite) are randomly translate to each other and rotate about the normal to the graphene layers.

Even though conceptually CB is referred to as microcrystalline structured material, it is more suitable to describe using the term “aggregate”. The aggregate refers to the chaining and clustering of CB particles or simply defined as the small dispersable unit composed of extensively coalesced particles. Burgess et al (Burgess et al) redefined the terminology and named CB aggregates as a “paracrystalline unit”.

CB particles are small spheroidal shaped and non-discrete components of an aggregate. Only by a fracturing, CB particles can be separated from aggregates. Sometimes, the term agglomerates are also used to define CB. The agglomerates are comprised of large number of aggregates. Aggregates are physically held together in agglomerates while particles are linked together as continuous graphitic structure within aggregates. Forces that bind particles together within the ‘aggregate’ structure of CB are those of chemical bonds. Such chemically binded aggregates are called as ‘agglutinates’.

Particle size, aggregate size and shape vary with respect to different grades of CB and its different manufacturing processes. These sizes and its distribution within CB define the end use application of CB. Apart from these size measurements and understanding, surface area is an important property which defines CB grade classification. The surface area measurements and its influence will be discussed more in chapter 4.

Another parameter which defines the quality of CB is its pore size. Theoretically, microstructure and formation of CB is easily understandable by defining porosity of CB. Porosity can affect surface area measurements. It can also be used to increase effective loading of the CB and influence certain application and properties of CB.

The particle size, aggregate size, morphology and microstructure of CB influence the properties of CB. The nature of CB surface, its porous structure, surface area and its chemical composition are the vital important factors which makes CB to use in wide

range of application i.e., mechanical, electrical, electronics, electrochemical applications etc., An amorphous structured materials are usually have high resistant to wear. Due to CB's characteristics when used as filler material enhances the tear strength and improves modulus and wear properties of tires, nearly about 90% of CB produced worldwide is used by the tire industry [21].

2.3. Structure of graphite, graphene and nanotubes

In a graphite, one of the 2s electrons hybridizes with two of the 2p electrons and forms three sp^2 orbitals at 120^o to each other in a plane. The remaining p_z configuration placed in 90^o to this plane. In graphite, three electrons in each carbon atom use to form simple bonds to its three close neighbors. That leaves a fourth electron in the bonding level. These "extra" electrons in each carbon atom become delocalized and no longer associated directly with any particular atom or pair of atoms. Hence, they are free to wander throughout the whole sheet. Hence, the sp^2 orbitals forms stronger σ bonds between carbon atoms in the graphite sheet. The p_z or often called as π orbitals provide weak vander Waals bond between the plane.

The structure showed in Figure 1 is called as Bernel graphite named after first proposed by John D. Bernel in 1924 [24]. Ideally, a less perfect graphite structure, an interplanar spacing value is ~ 0.344 nm. This value is significantly larger than the value for single crystal graphite. The carbon –carbon separation in graphite is about 0.142 nm. The in-plane C-C bond is very strong and hence the in-plane lattice constant is quite stable against external perturbations. At the same time, the nearest-neighbor spacing between carbon atoms in graphite is very small.

The noble prize winner of 2010, Andre Geim and his colleagues used an amazingly simple technique which involved rubbing a freshly cleaved graphite surface against another surface and finally isolated individual sheets of graphene. Graphene is a one-atom thick planar sheet of sp^2-bonded carbon atoms and are densely packed in a honeycomb crystal lattice. Graphene is the basic structural element of some carbon

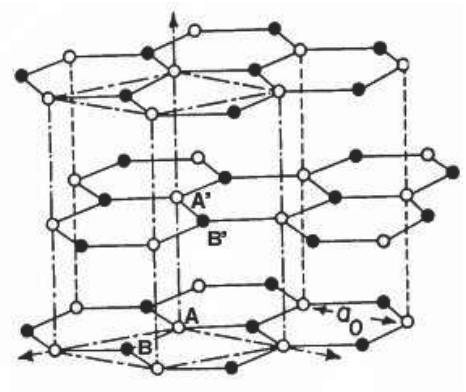

***Figure 2.1**: The crystal structure of hexagonal single crystal graphite. Reference: [33].*

allotropes including graphite, CNTs and fullerene. Carbon-carbon bond length in graphene is about 0.142 nm as like in graphite.

Interestingly, it was immediately attracted towards a wide range of electronic application due to its peculiar electronic properties. Electrons in graphene behave like massless relativistic particles since they obey a linear dispersion relation and hence graphene opened new perspectives of carbon-based electronics [25]. A number of graphene layers are rolled to form multi-walled carbon nanotubes (MWCNTs).

Graphene and CNTs are useful in nano electronic devices and nano field emitters due to their inherent and excellent electronic properties because of their nanoscale nature. The main areas where nanotubes find its applications are: ultimate reinforcement fibers for composites, field emitters (individual nanotube field emitters, large area flat panel displays,); nano tools (tips for scanning tunneling, atomic force, magnetic resonance force and scanning near-field microscopes, optical/chemical/biological force microscope tips, nano manipulators, nano tweezers).

Carbon Nanotubes (CNTs) are unique nanostructures. Ideal nanotubes are formed with graphene sheets rolled up into a cylindrical shape. Single CNT cylinder possesses diameters of the order of a few nanometers and length up to some millimeters with at least one end capped with a hemisphere of the fullerene structure that is six pentagons. CNTs are classified into two types i) Single-Walled Carbon Nanotubes (SWCNTs) and ii) Multi-Walled Carbon Nanotubes (MWCNTs).

SWCNTs consist of a single sheet of graphene rolled in around itself (like a rolled up newspaper) and MWCNTs consist of multiple layers of graphene arranged in

concentric cylinders (like a Russian Doll). The way the graphene sheets rolled determine the fundamental properties of the CNTs. Iijima initially observed MWCNT [26] and later in 1993 he was able to synthesize SWCNT and elucidated its structure [27].

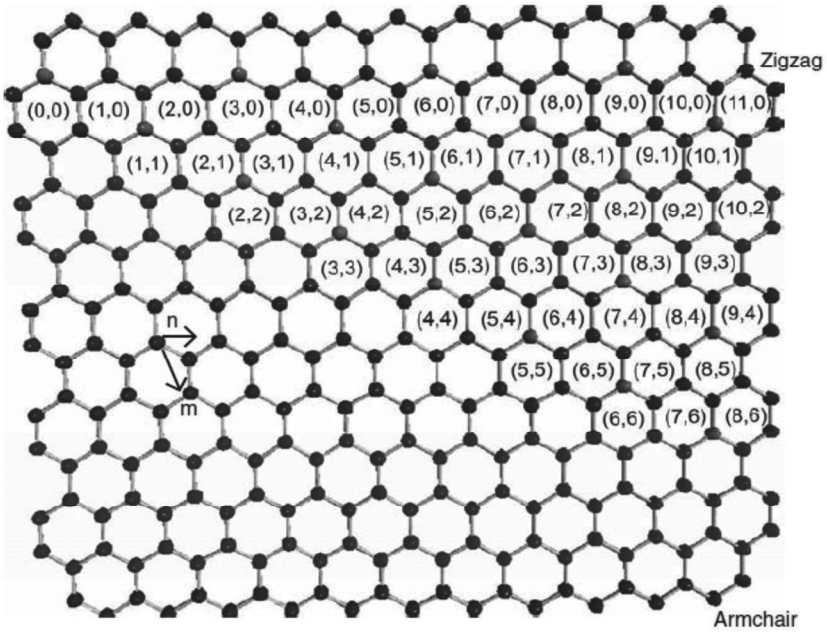

***Figure 2.2**: Single Graphene layer of CNT with atoms labeled using (n, m) notation. Reference: [37].*

A graphene layer illustrating (n, m) notations [28] is showed in *figure 2.2*. A CNT is normally described by a pair of (n, m) indices and which denotes the way the graphene sheet is wrapped to form a nanotube. The integers n, m gives information about the number of unit vectors along the two directions in graphene's honey comb crystal-lattice as indicated in the *figure 2.2*.

The stacking arrangement of the nanotubes is similar to the graphene sheets in turbostratic graphite. Perfect nanotube cylinders are at a large spatial separation from one another and thus should be able to slide past one another easily. A significant property of CNT is its electronic structure of turbostratic graphite, a zero gap

semiconductor, a semimetal with a small band overlap (0.04 eV) and this makes a qualitative difference from that of ideal graphite.

The easiest way to denote the structure of an individual nanotube is in terms of vector C, joining two equivalent points on the original graphene lattice. As discussed above, a cylinder is formed by rolling up the sheet, meaning that the two end-points of the vector are superimposed and because of the symmetry of lattice structure, cylinders are described in equivalent. That is, as all the carbon atoms involved only in hexagonal aromatic rings, they are in equivalent position. Equivalent nature varies only at the nanotube tips, where $6\times5 = 30$ atoms are involved in pentagonal. The chemical reactivity in the case of an ideally perfect SWCNTs will therefore be highly favored at the tube tips [29].

As carbon atoms are bonded in an aromatic ring structure, ideally the C=C bond angles have no longer ideal planar structure [29]. This means that the hybridization of C atoms get some percentage of the sp^3 character and are no longer complete sp^2. This varies in a proportion that the percentage of sp^3 character increases as the tube radius of curvature decreases.

Zig-zag and arm-chair are the two possible high symmetry structures for nanotubes. These two structures, as illustrated in *figure 2.3* in this thesis [28], represents with respect to the nature how the nanotubes are rolled. Naturally CNTs do not exists with the high symmetry structure and are generally in the chiral form. It is given the name ‘Chiral’ as they can exist in two-mirror related forms. The name “Helical” should be given to denote this type of nanotubes, however, in order to respect the definition of chirality, which makes all chiral molecules unable to be superimposed on their own image in a mirror, ‘Chiral’ is used [29].

The chiral angle is used to separate carbon nanotubes into forementioned three classes and they are all differentiated by their electronic properties. The pair of integers (n,m) represents a possible tube structure. The various ways to roll graphene into tubes are thus mathematically formulated by the vector **C** :

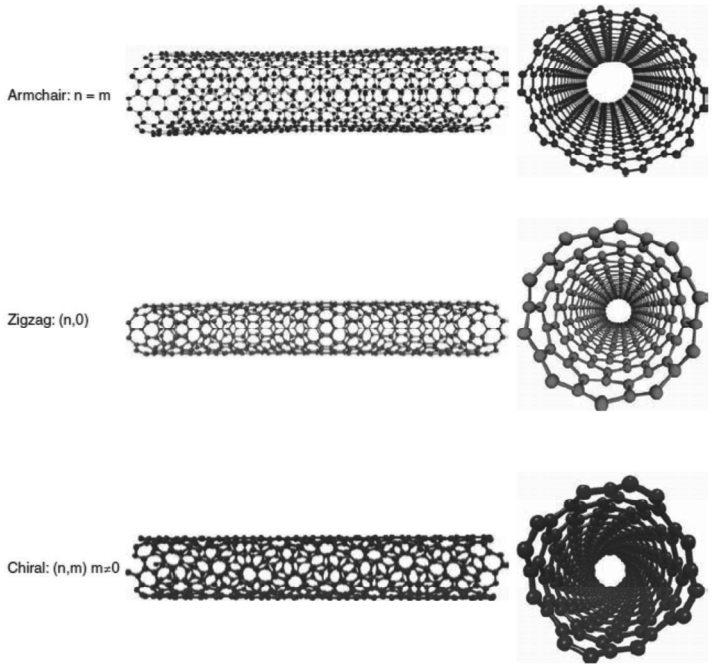

***Figure 2.3**: Examples of three types of nanotubes with (n, m) notations. Reference: [37].*

Where, a_1 and a_2 are the unit cell base vectors of the graphene sheet, and $n \geq m$. In armchair type, $n = m$, $\theta = 30°$, and in zig-zag type, $m = 0$, $n > 0$, $\theta = 0°$, and in chiral tubes, $0 < |m| < n$, $0 < \theta < 30°$. Armchair carbon nanotubes possess metallic character (a degenerate semimetal with zero band gap) and Zig-zag and chiral nanotubes can be semimetals or semiconductores. Semi metallic nanotubes are exist with a finite band gap, if $n–m/3 = i$, where i being an integer and $m \neq n$, and in all other cases semiconductor nanotubes exists.

Since its first observation by Iijima [26], a number of methods such as pyrolysis, plasma enhanced or thermal chemical vapor deposition, laser vaporization, ball milling of graphite, decomposition of C_{60}, rapid thermal processing, and annealing of soot have been used in synthesis of carbon nanotubes [30-41]. Each method has its

own unique features and nanotubes synthesized using different methods have shown a wide variation in morphology and properties.

The synthesis methods that operate in temperatures higher than 1000 °C do not often require presence of any catalyst. On the other hand, when the temperature is lower, then it is highly important to choose an appropriate catalyst usually in a form of metal nanoparticles. In all the catalytic synthesis methods, the type and size of the catalytic metal nanoparticles have turned out to be important factors as they control the formation process, shape and diameter of the nanotubes [37, 40, 42].

There have been also a few reports successfully transformed CB into nanotubes and other graphitic nanostructures [15, 22, 43-46] via catalytic and non-catalytic processes.

The synthesis of CNTs using chemical vapor deposition (CVD) has a number of advantages compared to other techniques. However, there are some disadvantages concerning safety, contamination and cost. When using hydrocarbons, great care must be taken to avoid back pressure due to hydrogen production during decomposition of hydrocarbons. Also possible complexity in chemical reaction and its products must be studied and precautions to be taken accordingly.

This project uses carbon black (CB) as carbon source instead of the traditional choice of hydrocarbons. Experiment of synthesizing CNT from CB is simple compared to the traditional approach. In the synthesis of nanotube structures, metal-filled and metal encapsulated structures can also be produced when organometallic compounds are used. In metal-encapsulated carbon nanostructures, carbon shells act as a barrier against oxidation and thus protect the metals. Further, mechanical, electrical, thermal and magnetic properties of the carbon nanostructure get altered with the encapsulation of metals [14, 47].

Chapter 3

Modification reactions on carbon black

This chapter summarize the studies on the literatures related to both the projects, i) solid-phase transformation of CB into graphitized nanostructures and ii) chemical modifications of CB using di-carboxylic and tri-carboxylic acids.

3.1. Solid-phase transformation of CB into graphitized nanostructures

The studies on the solid-phase transformation of carbon, such as from diamond, CB, activated carbon, glassy carbon, fullerenes to graphite (graphitization) and the structural modification or re-arrangements of less ordered graphitic stacks into more ordered layers etc., have been carried out since many years and their kinetics and phase transformation mechanisms have been derived [6, 9, 48-55].

The transformation of amorphous carbon into graphitized carbons was tried out by many researchers and the carbons were even classified in terms of graphitization, graphitizable, non-graphitizable and intermediate, i.e. partially graphitized carbons [48, 56-59].

The solid-phase transformation process of CB particles is carried out in the quest of obtaining further insight into the carbon structures [55]. The structure of the graphitized particles resulting from CB by means of transformation process (catalytic/non-catalytic heat treatment, laser irradiation, e-beam irradiation etc.,) depends mainly on the nature of the original CB [49, 55].

Marsh et al [60] carried out X-ray diffraction (XRD) studies on CB, after having heat treated the samples to high temperatures, to investigate the structural changes, and reported that many bent and faceted layer planes and few closed shell structures would be formed. However, CB cannot be fully graphitized by high temperature heat treatment as it does not possess any crystal nucleus for pentagonals and hexagonals to

grow around [22]. Formation of fullerene-like structures within CB particles during heat treatments is possible, nevertheless they grow in a random and disordered fashion as reported elsewhere [61-64].

High temperature treatments were carried out which transforms CB into bent and faceted particles that sometimes appear to have closed shell-like structures [55, 60]. Sometimes heating to high temperature by either arc-discharge treatment or laser irradiation, transform CB into graphite, nano-onions, or nanotubes. The transformation of CB into CNTs by low temperature treatment with the use of a metal catalyst is also possible, and electron bombardments have also been reported to transform CB into nanotubes, nano-onions, nano-diamonds, and C_{60}.

High temperature treatment called 'graphitization' is used to improve the crystallinity of CB. In such methods, CB is heated above 3000 °C to attain graphitic transformation. The rate of transformation or yield however depends on the nature of the original CB [55]. In some cases, the resulting graphitized CB have resulted with relatively large, discrete particles while in other cases the graphitized CB have a less well-defined structure with many bent and faceted layer planes and some apparently closed shell structures. A few researchers suggested that these faceted and closed ring structure in the heat treated carbon gives evidence that the original structures contain pentagonal rings [60, 65]. However, this argument is not completely agreed upon as the pentagonal rings might have formed during the heating process.

Sometimes, a high-resolution transmission electron microscope (HRTEM) is used for CB transformation. An irradiation with an electron beam focused to a current density as high as 150 A/cm^2 converts CB into carbon nano-onions. Irradiation with high current density is a faster process than the high temperature treatment process. Electron beam irradiation is more successful in graphitic conversion than high temperature because in high temperature treatments, agglutinations remain unchanged and conversion into fullerene-like structures or nano-onion like structures is possible with voids in the centre. In electron beam irradiation process, on the other hand,

agglutinations are completely destroyed and primary particles are graphitized without any voids.

Setlur et al. [66] reported that the heat treatment of soot at 2200-2400 °C mainly resulted in the formation of nanoparticles. When the soot mixed with amorphous boron and the heat treatment resulted in the formation of nanotubes with several microns in length [66]. However, similar experiments, where soot was replaced by CB or ball milled graphite, did not result in nanotube formation. Even though Setlur et al. were not been successful in synthesizing nanotubes from CB, subsequent work showed the possibility of transforming CB into nanotubes [15, 67, 68].

Solid-state transformation of CB into MWCNTs has been carried out at the anode of a modified high-temperature arc-furnace without a catalyst [15]. It has been proposed that the migration of pentagon and heptagon defects present in CB to regions of high tensile-stress is key to the growth mechanism. The initial stage of this solid state conversion of CB into nanotubes is a transformation of the necks between CB particles into short nanotubes by thermal forces. Then, at the second stage, the extension of the short nanotubes to multiple-micron lengths, driven by the electrostatic forces present in the plasma of the high-temperature arc-furnace.

In addition to the graphitization process and structural transformation those usually occurs at high temperature or high energy radiation, relatively low temperature transformation of CB into nanotubes is also shown possible [44]. Kishinevsky et al. [44] presented a set of experiments at 700 °C using $Fe(CO)_5$ together with CB and obtained nanotubes. They concluded that the yield of CNT was less when using $Fe(CO)_5$ alone than when using $Fe(CO)_5$ together with CB as additional carbon source. The authors used C^{13} enriched carbon black and estimated that half of the carbon in the carbon nanotubes originated from the carbon black. They suggested that the carbon in the CB is accessible since CO_2 and carbon structures are in a dynamic equilibrium with CO.

Onion-like hollow carbon nanoparticles with diameter of 40 to 100 nm were generated when acetylene CB were heat treated at 1000°C for ten hours in the

presence of ferric nitrate in an electric furnace [69]. It was suggested that the turbostratic concentric graphitic layers were transformed from the reconstruction of discontinuous short fragments of carbon black by the iron-based catalytic graphitization.

In the present work, carbon black (CB) is used as the carbon source for the synthesis of nanotube along with two organometallic compounds (ferrocene and nickelocene) as the precursors for the catalysts. To point out an essential difference in our approach to previous approaches [15, 22, 43, 46] is that a simple and relatively low temperature transformation process at 1000 ºC with a low thermal heating rate (10 ºC/min) is performed.

As discussed above, a number of studies have been carried out earlier on the catalytic or solid-state transformation of amorphous or other carbon structures into nanotubes. Solid-state transformation of amorphous particles into nanotubes needs very high temperature almost equal to graphitization temperature. Catalytic transformation of amorphous particles into nanotubes however uses relatively low temperature compared to solid-state transformation, but results in poor quality of nanotubes [44] or in only carbon nano-onions [69], or ends up with partial graphitization. Those processes either consume a lot of time or energy, or require complex cleaning processes of the products and/or equipment after reactions. Catalytic transformation processes carried out so far either used stainless steel as substrate or used oxygen during the reaction or as a precursor [22, 44, 46]. The present work aims at reducing energy and time consumption and carries out catalytic transformation of CB into CNTs at relatively low temperature.

In addition, in the present studies, the catalyst source and carbon source are loaded together in a ceramic boat and kept at a fixed position inside the chamber. Hence, uniform temperature is maintained in the reaction boat throughout the process. When using hydrocarbon or other gases as a carbon source, it would be set to flow inside the reaction chamber only at high temperature. The temperature inside the chamber varies a lot, with a maximum temperature at the center and a relatively low

temperature at the inlet and outlet. The input gas must pass through the zones where temperature is varied in each zone. Hence, chance for the contamination is more likely possible in such methods. Some studies used a double zone furnace in order to avoid contamination. In that type of synthesis process, decomposition of hydrocarbon takes place in one chamber and the products will be taken to a second chamber by the carrier gas. In the second chamber, the catalytic synthesis of nanotube is carried out. This again increases the cost of equipment and complexity of the whole process. In the present work a single zone furnace is used.

The role of catalysts is essential in the formation and growth of nanotubes since type and size of the catalysts can control both the formation process and the diameter of the synthesized nanotubes [42, 70]. Nano-sized particles of iron-group metals (such as Fe, Ni and Co) are well known for their catalytic activity in the synthesis of CNTs [30, 70-74]. These metals have unique interaction with carbon materials since the d-orbitals of the transition metal and the p-orbitals of carbon tends to overlap easily, and are known to show the highest ability of carbon diffusion [22]. In these types of metal-assisted syntheses, the diffusion of carbon through the metal particle(s) as well as the segregation of the diffused layer in the form of ordered graphene layers have been suggested as key processes in the growth mechanism of carbon filaments and nanotubes [75].

We also studied the effect of catalysts in the transformation process. In nanotube synthesis via hydrocarbon synthesis, the role of bimetallic alloy particles of transition and other metals, such as Ni–Fe, Fe–Co, M–Cu and M–Al (where M represents the transition metal), have been extensively studied [71, 74, 76-81]. These bimetallic catalysts have been found to show excellent catalytic properties in the synthesis of nanocarbon products, exceeding those of the mono-metallic catalysts. In particular, the use of Ni-Fe alloy catalysts for nanotube synthesis leads to a larger yield compared to the case when either pure Fe or Ni is used [82, 83]. We investigated here the role of both mono-metallic and bi-metallic catalysts in the structural transformation of CB into graphitized nanocarbon products. It is interesting

to note that the range of crystallinity and the rate of yield varied with the total amount of bimetallic catalysts.

In addition to the well-known iron-group metal catalysts, use of catalysts such as Au, Cu, Ag, Pt, Pd, and Al [75, 84, 85] are also reported to yield CNTs in spite of their low ability of carbon diffusion and negligible carbide formation [70, 86].

3.2. Chemical modifications of CB

CB can be used for diverse applications without further modification of its properties. Nevertheless, many researchers have tried to modify the surface of CB for e.g. electrical and electronic applications, sorption applications, improved coating performance etc. CB is frequently used as catalyst support in fuel cells due to its relatively high stability in both acidic and basic media, good electronic conductivity and high specific surface area [1-5]. The CB surface can be easily modified by introducing functional groups. Since unmodified CB sometimes reveals inadequacies for energy applications, nanocarbon materials can be modified at the micro- and nanoscopic level.

Compared to other nano materials, CB possesses high specific area and good electronic conductivity and has relatively high stability in both acidic and basic media. Because of this quality, CB is frequently used as a catalyst support [11]. The modification of CB at the micro- or nanoscopic level have strong influence on their reactivity in the reaction medium and the catalytic properties can be modified and improved [13]. Chemical or surface modifications of CB have been done in order to improve the properties of anchoring the nanoparticles/electro catalysts.

By functionalizing the surface of CB, one alters the surface properties, and the hydrophilic or hydrophobic character of the surface may change according to the chemical nature of the surface groups. Surface reactivity and polarity (zeta potential) may also be altered. Surface modifications of CB have mainly been performed with the intension of developing new materials for diverse applications like coatings and

ink. In addition, grafted components may provide nucleation sites for deposition of highly dispersed metal particles yielding potential materials for fuel cell catalysts with increased activity [11-13].

Earlier, reactions such as oxidation (e.g. with mineral acids, potassium sulfate, H_2O_2, anodic oxidation), polymer grafting, esterification or Friedel-Crafts reactions have been used to modify the CB surface. Oxidation of CB surfaces has been carried out for years to study the effect on the surfaces and on the interior carbon structures [87-92]. In some studies, oxidations were performed on carbonaceous products at elevated pressures, recovering oxalic and aromatic acids as the product [93]. Experiments have also been carried out to study structural changes and surface groups of CB after oxidation with nitric or sulfuric acid, and H_2O_2 [11, 94-97].

Functional groups such as hydroxyl (–OH), carbonyl (-CO), sulfate ($–OSO_3H$), carboxyl groups (-COOH) have been found to be introduced on the surface of CB when the carbon is reacted with HNO_3 [11, 90, 92], $KMnO_4$ [98], H_2SO_4 [97], H_2O_2 or ozone gas (O_3) [95, 99]. The functional groups attached to the surface of CB provide nucleation sites for the deposition of highly dispersed metal particles. These surface oxidation methods are not simple and usually require extensive heating (usually 4–48 h), filtration and washing to remove the oxidant. Some researchers have used oxygen plasma for modification of CB which introduced oxygen functional group onto its surface, and this showed improvement in wetting behavior [100, 101]. Chemical reactions could be applied to encapsulate, protect and change the hydrophobic/hydrophilic character of the materials.

However, the traditional oxidative methods are not easily controlled and the resulting carbon contains residuals. Therefore, recently, modification of the CB surface with carboxylic acids or their derivatives has been studied [12, 102, 103]. Treatment of carbon materials with unsaturated carboxylic acids or with their derivatives is simple and effective. In addition, it does not require prolonged heating, filtration and washing as it is required when using mineral acids. Poh et al. report on chemical modification of CB using citric acid [12]. They find that citric acid modified carbon

materials have more functional groups attached to their surfaces compared with acid refluxed carbon.

The second project deals with the chemical modification of CB surface with the intention to provide simple and effective reaction technique. Thus, we used carboxylic acid treatment to modify the surface and have studied different reactions with di-, and tri-carboxylic acids. As both the maleic and citric acid varies with the concentration of hydroxyl and carboxyl molecules, surface reactions on the carbon is expected to be different. The effect of solvents (water/ ethylene glycol) and the effect of pre-heat treatment of carbon have been studied. Both Timcal 350G and XC72R CB samples have been used in the chemical modification experiments. This work further studied the processes and shown the results varies with the solvent used and pre-heat treatments on CB.

Chapter 4

Characterization methods

4.1 Raman Spectroscopy

Raman spectroscopy is complementary to IR spectroscopy and plays a significant role in providing structural characterization of graphitic materials [104]. Raman spectroscopy is one of the standard non-destructive tools for characterization of crystalline, amorphous and nano crystalline carbons [104-115]. Its importance lies in the fact that it can detect even small changes in the structural morphology of nanocarbon materials.

The basic principle of Raman spectroscopy is based on an inelastic scattering of monochromatic light, usually a laser source. Inelastic means that the photons of the laser light when hitting the sample is absorbed by the sample and the re-emitted photons have energies lesser or higher than the original monochromatic light. This phenomenon is called Raman Effect and it is fundamental in Raman spectroscopy. The Raman shift provides information about the vibrational, rotational and other low frequency transitions in the molecules of the sample. The information can be obtained from the Raman spectrum: the scattered light is collected by the lens and sent to an interference filter, and the Raman spectrum is obtained which holds information about the sample's nature.

In this project, a Horiba-Jobin Labram 800 HR Raman spectrometer was used at the Centre for Geobiology, University of Bergen, Norway. Raman analysis was carried out on powdered samples placed on glass slides which were directly mounted under an Olympus BX41 petrographic microscope. Measurements were performed with a 100 mW, 514 nm Argon ion Laser, focused to beam diameter of 1-2 μm through a 100x objective. The spectrometer was re-calibrated before each analytical session by 'zero-point' centering, and analysis of a Si-standard with a characteristic Si Raman

band at 520.4 cm^{-1}. Spectra were obtained for 2x10 seconds in multi-window mode over a range of 800-3100 cm^{-1}, using an edge filter for 514 nm excitation wavelength with a 100 cm^{-1} cut-off, a 100 μm entrance slit, a 1,800 lines/mm grating, and a Peltier-refrigerated (-70°C) 1024x256 pixel CCD array detector. The effective laser power on the sample was nearly 0.5 mW.

From the Raman spectrum the following features can be determined:

A low frequency peak (<200 cm^{-1}) normally absent in graphite but present in SWCNTs is assigned to A1g symmetry radial breathing mode (RBM) [116]. The frequency of RBM is inversely proportional to the tube diameter (d) and hence can only be detected for d > 2 nm.

Raman spectra can be used to identify the carbon materials. For example, in the first-order spectrum (<1700 cm^{-1} range), Diamond shows single peak at 1332 cm^{-1}, while commercial grade graphite such as multi crystalline graphite shows a sharp peak at 1355 cm^{-1} [105], while other kinds of amorphous and nanocrystalline carbon displays peaks at 1360 cm^{-1}[117].

Raman shift at 1350 cm^{-1} (D1-peak) and 1620 cm^{-1} (D2-peak) represent vibrations associated with the A_{1g} breathing mode of sp^2-hybridized carbon rings while the shift at around 1580 cm^{-1} (G-peak) represents E_{2g} bond stretching of hexagonal ring structures that make up graphite [106, 110]. This vibration becomes possible in ‘disordered’ or nano-crystalline structures where the in-plane crystal domain size is limited by lattice defects. G and D1 peaks of varying intensity, position, and its widths plays a major role in the analysis of amorphous and nano crystalline carbons [115]. The presence and intensity of D1 and G peaks at 1350 cm^{-1} and 1580 cm^{-1}, respectively are used commonly to describe the quality of nanotubes. The G peak is the best defined peak for carbon materials, as it is always present at any excitation energy and for any carbon [107].

The second order Raman spectra at 2450 $cm^{-1}$and 2950 cm^{-1} are specific bands that appear only for disordered carbon and nanostructured carbons. Second order

spectrum is highly sensitive to the degree of graphitization and structural changes in carbon related materials [109]. The peak at ca. 2705 cm^{-1} (G'-peak), however, represents the second harmonic of the D1-peak in nano-crystalline graphite. This band is symmetric and very intense relative to the first-order G-band in single layer graphene or thinly stacked graphitic structures [113-115, 118], while in pure crystalline graphite it is typically less intense and splits into two separate peaks [113]. It should be stressed that a relatively intense 2700 cm^{-1} band is also observed in certain natural carbonaceous materials [119], and has been attributed to the presence of turbostratic graphite or to the presence of carbon crystallites with highly variable dimensions.

In the carbon nanostructures, the ratio of the intensity of D-line (ID) to the intensity of G-line (IG), ID/IG increase with increasing structural disorder, that is, ID/IG is regarded as a CNT morphology indicator. Low ID/IG values are assumed to denote well-graphitized CNT. The intensity- or area-ratio of the D1- to G-peak varies inversely with the in-plane crystal domain size (La) of various graphitic materials [110, 114].

4.2 Scanning Electron Microscope (SEM)

SEM is one of the important tools compared to other tools commonly used for characterization of morphology, dimensions and structure of nanoparticles and nanotubes. It has two major advantages over the optical microscopes, i) resolution and ii) depth of field. It is possible to obtain three-dimensional images of nano-scale sized materials with high-resolution. Among other electron microscopes (such as transmission and high-resolution transmission electron microscopes, TEM and HRTEM), operation and analysis of results are simple in SEM. SEM is important in analyzing the purity of carbon nanomaterials, as it allows quantifying the percentage of unwanted substances per unit area within the sample [116].

Depending on the source of the electron, SEM can be classified into two main types, thermionic emission SEM and field-emission SEM. In thermionic emission type, the filament (eg. tungsten) is connected to a source of current and electrons are passed through it. Hence filament heats up and finally electrons start to emit. In this type of gun, both the outside source of electrons and the heating source are one in the same. In the field emission type SEM, the electron gun uses a finely tipped tungsten crystal. Instead of being heated and draw electrons as in a thermionic emitter, an intense potential field on an anode that lies beneath the tip of the filament is used to draw electrons. Throughout this project, field-emission SEM is used.

The resolution of SEM is about 1.0-3.0 nm depending on the accelerating voltage, which is typically varied from 1 to 30 kilovolts (kV). For a high-resolution mode, the magnification can be varied from 100 to 650,000 times and for a low-resolution mode, it can be varied from 25 to 19,000 times. For example, SEM instrument, Supra 55V of Zeiss microscopy can achieve resolution of 1.5 nm to 0.5 nm when used between accelerating voltage of 1 kv to 20 kv. A moderate vacuum is needed in the SEM column and in the sample chamber. Vacuum facilitate the electrons to travel freely from the electron beam source to the sample and then to the detectors. Higher vacuum, typically 10^{-5} to 10^{-7} Torr is needed for obtaining high-resolution images.

Overall diameters of CB nanoparticles and CNTs can be estimated using SEM, TEM, and HRTEM images; however, SEM is limited when it is needed to study inner morphology of carbon nanomaterials [116].

4.3 Transmission Electron Microscope (TEM)

TEM is a classic analytical electron optical instrument and was first constructed in 1931 and the first commercial TEM was built in 1939 [120]. The major advantages of TEM are i) its high lateral spatial resolution (better than 0.2nm) and ii) capability of giving both image and diffraction information from the same sample [120].

TEM works with a typical accelerating voltage of 100-200 kV. Some commercially available TEM works in high-voltage, 200-400 kV. An additional advantage of using high-voltage TEM is its greater electron penetration. High energy electron interacts less strongly with matter than low energy electrons and hence, it is possible to work with even thicker samples.

In SEM electrons return from the surface of a bulk are used for the image formation.

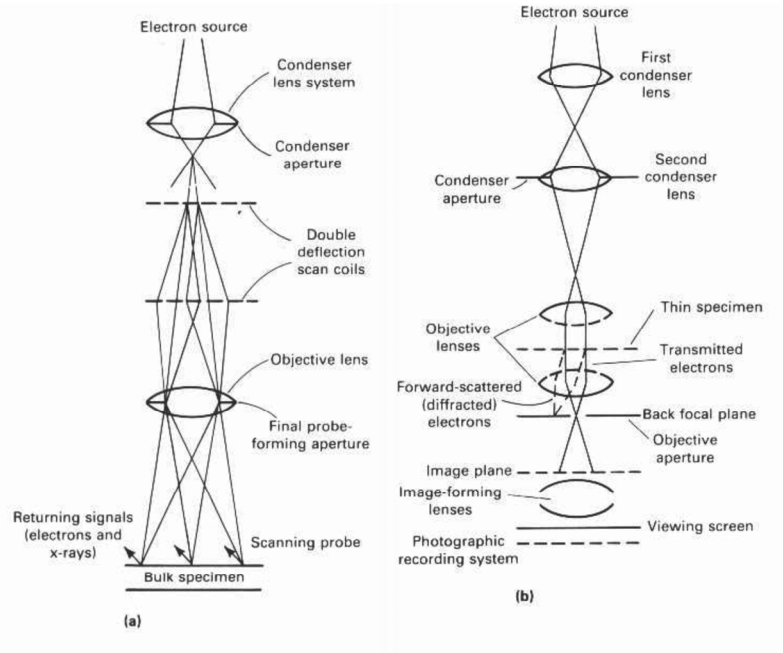

***Figure 4.1**: (a) showing schematic diagram of SEM and (b) showing schematic diagram of TEM. Ref: [127].*

SEM image gives information about the specimen morphology, surface structure and chemical composition of the samples. In TEM, electrons penetrate a thin sample region and image is formed at the lower section of the instrument. TEM looks into the internal structure of the samples, crystal structure and chemical composition as well. In TEM, electron beams emitted from an electron gun incident on the thin sample (typically cu grid). Both deflected and undeflected electrons that penetrate the sample thickness gives rise to signal as output.

From the images obtained using low magnification TEM, it is possible to quantify the number of tubes and other objects of irregular shapes per unit area, as like in SEM, and can estimate the purity of the samples.

The resolution limits in the conventional TEM are exceeded by the high-resolution TEM (HRTEM). Nowadays, HRTEM has resolving powers at or close to one angstrom (1 Å). High resolution images are interpretable to very high resolution by using correct operating conditions and well-prepared samples. The images are recorded directly in terms of projections of individual atomic-column positions, and atomic arrangements at defects and other homogeneities can be accurately determined by the HRTEM. Further individual graphite layer in primary carbon can be observed and provides information about the arrangement of graphitic layers. In particular, related to carbon materials, imaging of 002 lattice fringes of graphite-like substructures is possible by HRTEM, thereby it a direct view inside a primary carbon particle can be derived [121].

In the analysis of nanotubes, it is actually a complementary tool to view the way the tubes are arranged (for ex, whether the tubes are concentric, stacked cup arrays, herringbone, and bamboo or nested). In addition, HRTEM is highly useful in estimating the inner and outer diameter distributions of the concentric tubes [122, 123]. This project used JEOL 2100 TEM instrument and JEM 1230 HRTEM instrument for the sample characterization. Prior to TEM and HRTEM analysis, the sample was sonicated with ethanol and dropped into a copper grid.

The schematic diagram illustrating the differences of SEM and TEM is shown in figure 4.1[124].

4.4 X-ray diffraction (XRD)

X-ray diffraction (XRD) is also a non-destructive characterization method. With the use of XRD, crystalline phases of unknown samples, orientation of single crystals, stereographic projections, lattice parameters, weight fraction of crystalline phases in multi-phase materials etc., can be identified and measured. XRD is one of the early

studies used to determine the structural properties of carbon and led the way to determine the approximate data on interatomic distances [23, 125-128].

Warren in 1934 was first to study CB using X-ray diffraction and showed the presence of graphite-like structure of in a non-crystalline carbon [125]. XRD patterns of CB further studied by few researchers (1941 and 1942) and showed that it is composed of (001) three-dimensional and (hk) two-dimensional reflections [23, 126], and later confirmed that the three-dimensional structure of crystalline graphite is absent in CB as there is no trace of (hkl) (1≠0) graphite lines [48]. From the (002) peak in XRD, the interlayer spacing d002 can be directly found and is used to define degree of graphitization.

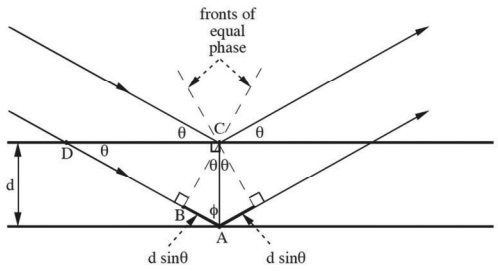

***Figure 4.2**: The geometry for the interference of a wave scattered from two planes separated by the interplanar distance, d.*

X-rays are an electromagnetic radiation typically in the range of 100eV- 100 keV photon energies. Only a short wavelength x-rays in the range of a few angstroms to 0.1 angstrom (1–120 keV) are used for a diffraction applications. The wavelength of x-rays is comparable to the size of atoms, and hence they are ideally suited for probing the structural arrangement of atoms and molecules in a wide range of materials.

In a XRD, X-rays when incident on the sample, primarily interact with the electrons in the atoms. The diffracted patterns were produced from the interference of diffracted waves arise from different atoms due to electron-atom interactions. These patterns can be used to deduce the distribution of atoms in the material. The diffraction angle, interplanar distance (d), can be measured based on the Bragg's law. The figure 4.2 shows the construction to derive Bragg's law.

Bragg's law for diffraction is $n\lambda = 2d \sin \theta$. Where λ is the wavelength of an incident x-rays, θ is an angle of diffracted x-rays.

In a XRD system, the diffraction pattern is collected by varying incidence angle of the incoming x-ray beam by θ and the scattering angle by 2θ. These two angles thus have to be varied during a $\theta/2\theta$ scan. In this present work, for the characterization of nanoparticles and nanotubes, the samples were fixed while both the x-ray source and the detector rotate by θ simultaneously.

X-ray powder diffraction techniques usually require some sample preparation. First, samples need to be crushed to fit inside a glass capillary tube or packing it into a sample holder of a certain size. A diffraction pattern can be recorded using film, analog, or digital methods. As discussed above, a set of peaks will be obtained as a result in XRD and this peak patterns are used for identifying unknown crystals in a sample material. This can be done by matching the position and intensity of obtained diffraction peaks to a known pattern of peaks.

XRD characterizations were carried out in this project using Bruker advanced XRD system, operated at 45 kV and 40 mA with monochromatic copper Kα1 radiation of wavelength (λ = 1.540598). The samples were loaded as a crushed powder into the sample holder and the characterization was carried on.

In this project, XRD is used to characterize the chemically modified CBs and CNTs and compared with that of parental carbon. XRD provides information about the structural arrangements of CB and also provides information about the structure modified after chemical treatments.

When CNTs are characterized using XRD, it provides phase information about graphitic structure, metal carbides and metal alloys.

With the results of XRD peaks, the determination of a graphitic structure and its phase, and the existence of metal carbide structures are possible. With the XRD peaks and its measurement of full width half height (FWHH) maxima of the particular peak,

it is easy to calculate the size of crystallites. From Scherrer equation, the crystallite size along the c-axis, L_C, is determined from (002) reflections, peak at around 26°.

$$L_C = \frac{K\lambda}{\beta \cos\theta}$$

in which K is the so-called Scherrer constant (K=0.89), λ is the X-ray wavelength (λ=0.154 nm), β is the full-width at half-maximum of the peak, and θ is the Bragg angle.

4.5 Fourier transform infra-red spectroscopy (FTIR)

Once it was considered difficult to obtain molecular level information on the carbon surface. This was overcome with the introduction of the characterization technique, infra-red spectroscopy (IR) [129]. The problem such as poor transmission, and uneven light scattering related to carbon nanoparticle size had been dealt by the introduction of diffuse reluctance Fourier transform IR spectroscopy (FTIR). This tool becomes powerful having advantages such as being non-destructive, mechanically simple, offering high resolution, and high speed in collection of spectra.

FTIR spectroscopy determines the changes in the intensity of a beam after it interacts with the sample. The intensity is calculated with respect to the wavelength or frequency (4000-200 cm^{-1}). The central part of FTIR spectroscopy is the infrared interferometer whose function is to disperse the light which comes from the infrared light source and to measure its intensity at each frequency. Finally infrared spectrum is drawn as a plot of the ratio of the intensity before and after the light interacts with the sample versus frequency.

Even though CB is difficult to characterize using FTIR, analysis was done to possibly identify any surface groups that might be created after chemical modification.

From FTIR spectra of CB surfaces, various details can be noted. The bands at wave numbers 1700-1300 cm^{-1} indicates the presence of carbonyl or carboxyl groups and

the bands around 1460-1420 cm^{-1} are often attributed to the OH in-plane deformation mode of the hydroxyl part of a carboxyl group. The peaks above 3000 cm^{-1} indicates hydroxyl groups in alcohols or phenols. C-H bonds have stretching modes around 3200 cm^{-1}. The bands in the region around 1550 cm^{-1} denotes C=C stretching vibrations in aromatic ring structures.

In this project FTIR has been used only for the analysis of chemically modified CB surface. The spectra were recorded using a Nicolet Impact 410 FTIR spectrometer. Prior to the analysis, the samples were dried and dispersed in spectroscopic grade KBr pellets.

4.6 Thermal gravimetric analysis (TGA)

Thermal gravimetric analysis measures physical changes in a material as a function of temperature. In this project, chemically modified CB samples were analyzed to study the changes created after reactions of CB with organic acids.

In TGA, a continuous measurement of the weight of a sample as a function of temperature is performed. CB samples were placed in a small pan connected to a microbalance and heated in a controlled manner and/or held isothermal for a specified time. The atmosphere around the sample consists of synthetic air. In the beginning of the experiment, the program starts in an inert atmosphere and then later switch to air to complete the analysis. Weight changes are observed at specific temperatures which are correlated to volatilization of sample components, decomposition, oxidation/reduction reactions, or other reactions or changes.

TGA thermograms were obtained using a thermo-gravimetric analyzer (TG500, TA Instruments). The samples were heated from ambient temperature to 1000°C at a heating rate of 10°C/min with synthetic air as purge gas at 40 ml/min flow rate.

4.7 BET Surface area measurements

BET surface area analysis was performed using the Micromeritics TriStar II surface area analyzer. Before the analysis, all the samples were degassed in N_2 for 1 hour at 300°C.

Surface area measurements using BET theory was first proposed by Brunauer, Emmett, Teller in 1938 [130]. BET theory calculate surface area by determining the physical adsorption of gas molecules on a solid surface and by measuring the amount of adsorbate gas corresponding to a monomolecular layer on the surface. The temperature of liquid nitrogen is used for such measurements. Evaluation of nitrogen multilayer adsorption as a function of relative pressure using a fully automated analyzer is carried out for surface area calculation. The amount of gas adsorbed on the surfaces of the solid is measured by a volumetric or continuous flow procedure.

The technique also provides external area and pore area evaluations to determine the total specific surface area in m^2/g. These evaluations are important for studying the effects of surface porosity and particle size in many applications.

4.8 Particle size analyzer and Zeta potential

Hydrodynamic diameter distribution and distribution averages for the chemically modified CB samples in aqueous solutions were determined by dynamic light scattering. Hydrodynamic diameters were determined using a Zeta Nanosizer ZS from Malvern Instruments. CB particles were dialyzed into water and then transferred to a cuvette prior to the measurements. Scattered light was collected at a fixed angle of 90°. A photomultiplier aperture of 400 mm was used. The incident laser power was adjusted and a photon counting rate between 200 and 300 kcps was obtained. The final measurement was done using the measured and calculated baselines of the intensity autocorrelation function agreed to within +0.1% were used to calculate nanoparticle hydrodynamic diameter values. All the measurements were done in multiples of three consecutive measurements.

Zeta potential (ζ) values for the chemically modified CB samples were also determined with a Zeta Nanosizer ZS from Malvern Instruments.

Colloidal stability and surface morphology can be predicted using zeta potential measurements, and the experiments were carried out on the assumption that dilution has no influence on the surface charge of a particle. Electrophoretic mobility obtained after light scattering was used to calculate the mean zeta potential for each of the samples

4.10 Curie-temperature measurements

Materials possessing a spontaneous magnetization can be identified by determining the temperature at which the ordered magnetic state (ferro/ferri-magnetic) changes to a paramagnetic state. This second order phase transition is termed the Curie-temperature. The diagnostic method requires a thermally stable magnetic phase, implying that the magnetic material is not altered by heating to just above the Curie-point.

The Curie-temperature is determined from thermomagnetic curves as the temperature at which the curve possesses a maximum curvature. A continuous or abrupt thermally activated chemical or structural phase-change may erroneously be interpreted to represent a Curie-temperature. Consequently, we have performed thermomagnetic experiments by cycling to progressively higher temperatures in order to discriminate between genuine Curie-points (reversible inflexions) and irreversible inflexions reflecting phase-destructions.

Thermomagnetic curves were obtained on a PC-controlled, automatic-recording transversal Curie-balance. Magnetic fields varied between 200-600mT and heating/cooling rates varied between 15-20°C/minute. All experiments were performed in air at normal barometric pressure.

Chapter 5

Results and discussions

In this chapter, the results and discussions of the experiments related to the solid – state transformations of CB and chemical modification reactions on CB are discussed.

For the studies on the solid-phase transformation behavior of CB nanoparticles into different nanostructured products, three different experimental set ups were used: 1) thermal evaporation using ceramic boat and stainless steel as the substrate, 2) the effect of microwave irradiation on the transformation process and 3) experiments in tube furnace using closed quartz tube. CBs used in these experiments were Ensaco 350G provided by Timcal Graphite & Carbon and Vulcan XC72R provided by Cabot Corporation, hereafter referred as Timcal 350G and XC72R. The sections 5.1-5.3 discuss the experiments listed above.

And finally, results obtained in the chemical modification reactions are discussed in the section 5.4.

Each experimental setup and their results are discussed separately in the following summary.

5.1 Thermal evaporation using ceramic boat and stainless steel as the substrate

5.1.1 Experiments and background:

The experiments are conducted to perform structural transformation of CB into CNTs. The variation of catalyst ratio to CB, temperature, catalysts, and substrate in the experiments were carried out to explore in depth phenomena in the catalytic

transformation process. The experiments are all conducted as follows, unless otherwise stated: Organometallic compound(s) were added to CB with the prescribed weight ratio. Afterwards, 20 ml of toluene was added to the mixture and then subjected to ultrasonic vibration for about 15 min so that the whole mixture becomes homogenous.

Next, the mixture was loaded into an open alumina boat (8 cm long and 4 cm height)/ a closed cylindrical stainless steel cell (35mm dia, 50mm height) completely filled with alumina balls (4 mm dia). The boat/cell was then placed at the center of an alumina tube single stage MXITL horizontal furnace of 80 mm diameter, 1000 mm in length at room temperature. Afterwards, the furnace was set to reach prescribed temperature (at the rate of 10 °C/min) and the sample inside the furnace was heated for 6 hours at the set temperature. The whole reaction was carried out under nitrogen flowing at an atmospheric pressure condition. The furnace was set to cool after 6 hours at a cooling rate of 5 °C/min. Finally, the sample was collected out from the ceramic boat/the cell.

Generally the temperature in the furnace depends on the flow rate of the cold nitrogen and the exact location of the sample in the furnace. Therefore, in the present research, these parameters were tested and optimized before the experiments started.

After the experiments, all the samples were cooled down to room temperature and then treated with 8M HCl at 80 °C for 1 hour and afterwards kept at room temperature for 24 hours. Finally, they were filtered, washed with distilled water and dried at 110 °C

Here we explain the growth mechanism of carbon nanostructures from CB on a substrate in the presence of bimetallic catalysts. In the early stage of reactions, nickelocene and ferrocene decomposes into nickel and iron particles, respectively, in addition to atomic carbon and hydrocarbon species of various carbon numbers. Carbon atoms that decomposed from metallocenes would also take part in the nanostructure formation, as similar to the mechanism explained and verified by Kishinevsky et al. [44]. The effect of carbon in the reaction due to toluene and

ethanol is negligible as these would decompose at lower temperatures (less than 200°C) and their hydrocarbon compounds in the gaseous phase leave the reaction zone. Similarly, most of the compounds from ferrocene and nickelocene also possibly evaporate below 500°C.

5.1.2 Effect of substrate:

This topic is discussed in paper II [131]. The temperature used in the present experiment is 1000°C and the mixture was loaded in closed cylindrical stainless steel cell filled with alumina balls and all other parameters remain same as explained above.

Two organometallic compounds (ferrocene and nickelocene) were used as catalyst precursors. The reactions were conducted in stainless steel cell, which is a prominently used substrate in CB transformation [44, 46], with alumina ball as an additional substrate. To our best of knowledge, there are no published reports about the transformation of CNT using such combinations (catalysts precursors and two substrates together). The aim of this work is i) to study the effect of the substrate in the catalytic transformation of CB into CNTs and ii) to study the effect of the weight ratio of CB to catalyst in the transformation of CB to CNTs.

During the reaction, complete solid solubility of nickel and iron occurs at 912 °C [73]. Hence, the working temperature in the present work (i.e. 1000 °C) favors Fe and Ni particles to well intersperse with each other in the alloy and allows better dispersion of the active catalytic sites. Metal particles in the alloy structure would be composed of many catalytic centers that could act as nucleation sites that favor the growth of carbon nanostructures [14, 47].

At first, CB, ferrocene and nickelocene were weighed in the ratio of 1:5:5 (0.1g: 0.5g: 0.5g). Toluene (25 ml) was added as a solvent to the mixture and then the mixture was ultrasonicated for 15 min to obtain a homogeneous suspension. The mixture was transferred to a cylindrical stainless steel cell (35mm dia, 50mm height) completely

filled with alumina balls (4 mm dia). The cell was closed and placed inside a horizontal furnace (80mm dia and 1000 mm long) and heated to 1000 ºC.

In order to study the effect of substrate on the catalytic transformation of CB into CNTs, two different samples were taken to be exposed to further treatment. The

Table 5.1*: Summary of composition, treatment and source of samples, showing the effect of different substrates in the transformation.*

Sample Name	*CB:F:N (weight ratio)*	*Substrate*	*Description*
CN1	1:5:5	Stainless steel cell filled up with alumina balls	Material collected from the surface of alumina balls
CN2	1:5:5	Stainless steel cell filled up with alumina balls	Material collected from the lower part of stainless steel cell where the material is likely to have been in contact with both stainless steel and alumina surfaces
CN3	1:5:5	Stainless steel cell	Material collected from inside the stainless steel cell
CN4	1:1:1	Stainless steel cell filled up with alumina balls	Material collected from the surface of alumina balls
CN5	1:1:1	Stainless steel cell filled up with alumina balls	Material collected from the lower part of stainless steel cell where the material is likely to have been in contact with both stainless steel and alumina surfaces

alumina balls were removed from the stainless steel cell and the first sample, named CN1, was collected from the surface of the alumina balls. The remaining material in the stainless steel cell was collected and the sample was named CN2.

The diameter distribution of the nanotubes synthesized using bimetallic catalysts, depends on both the composition of the catalysts and the catalyst particle size [81, 132]. Comparisons of samples CN1 and CN2 reveal that the sample taken from the alumina surface (CN1) contains mostly well-developed nanotubes with few 'bamboo'-like structures while sample CN2, collected from the lower part of the stainless steel cell, contains both nanotube and nano-onion like structures. In our study, the experimental parameters remained the same and the samples were synthesized within the same cell in a single experiment. Even though one can expect slight compositional variations of bimetallic catalysts with respect to different locations within the cell, the wide variations in the diameter of CN1 and CN2 nanotubes cannot be attributed entirely to the catalysts. We believe the effect of substrate in which nanotubes were grown is the main reason for the wide variations in the diameter distribution of the nanotubes in the two samples.

This can be explained more precisely by the fact that the alumina substrate is more porous than the stainless steel wall and the size of the pores influence the diameters of the resultant CNTs as registered earlier by Ward et al [133]. However, the difference in quality between CN1 and CN2 nanostructures can only be explained after carrying out additional in-depth studies in the future.

As mentioned earlier, metal-filled and bamboo-like nanotubes (in figure 5.1) are observed within the CN1 sample, but CN2 does not contain different morphological tubes. In addition to the effect of catalyst (size and composition), the growth and morphology of carbon nanostructures depend on temperature, metal catalysts, chemical diffusivity of carbon into metal, reaction time, etc. It means, even within the similar reaction environment, that regional effect plays a major role in the determination of morphology of the nanostructures. When comparing the morphology of CN1 and CN2 (in figure 5.1 and 5.2), we strongly believe that the wide deviation

in the thermal conductivity of stainless steel and alumina plays a crucial role in the early stage of graphene layer formation at the catalytic site of the metallic particles. This will in return, affect the growth path.

Further, the substrate physically interacts with the metal nanoparticles (here Ni and Fe) formed upon decomposition from their organometallic compounds (nickelocene and ferrocene). The fact that a porous nature of the substrate influences the diameter distribution also has to be considered here [133]. Hence, the variations in the morphology of nanostructures and diameter distribution, which we have described between CN1 and CN2, are certainly induced by the effect of the alumina balls and stainless steel surface.

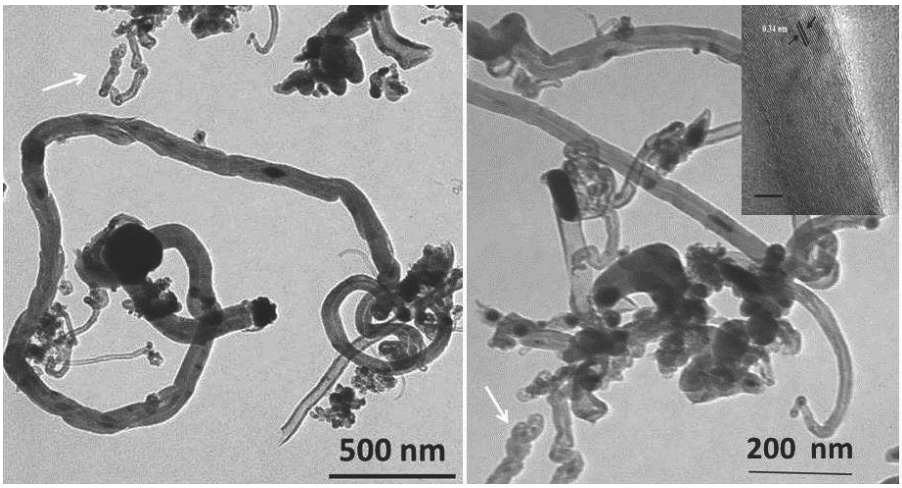

***Figure 5.1**: TEM (a-b) and HRTEM (inset in Figureure1b) images of sample CN1. TEM images indicating the formation of nanotubes with different morphologies and HRTEM image depicts the typical graphene layer arrangements in CN1 nanotubes. Refer [131].*

From TEM, HRTEM and XRD analysis to Raman analysis of samples CN1 and CN2 clearly confirm that these samples have completely different morphologies. It is noteworthy that synthesis of sample CN1 is likely to have been influenced only by the alumina balls whereas sample CN2 is influenced by both the alumina balls and stainless steel. However, assessing the relative influence of each of the substrates on

the produced structures is complicated since sample CN2 is likely to have been affected by both stainless steel and alumina surfaces.

From the overall TEM analysis of the samples CN1 and CN2, the length of the nanotubes obtained is found to be typically 1-10 μm. The length of nanotubes obtained in our work is much smaller compared to the length of the nanotubes transformed from CB by Buchholz et al. [15], which is about 100 μm and by Donnet et al. [46], which is 40-50 μm. The reason for such short nanotubes in our experiment may be explained as follows: hexagons must be continuously generated at the growing end of the tube in order to form lengthy nanotubes [15]. The tube end will be closed, that is the growth of nanotube stops with the formation of pentagons [134, 135]. Low flux density of carbon atoms is the possible reason for the formation of pentagons during growth of nanotubes and hence determines the tube length [46].

Thermomagnetic curves (illustrate in paper II [131]) during the three temperature cycles of samples CN1 and CN2 showed similar features. A well-defined inflexion point at ~350 °C during the first heating is diagnostic for pure nickel (i.e. 354 °C) and is interpreted to represent the catalyst. This magnetic phase disappears after heating to 500 °C indicating oxidation of nickel to a non-magnetic nickel-oxide. After a final heating to 700 °C, the weak inflexion point just below 600 °C indicates the presence of magnetite (580 °C is the Curie point temperature of magnetite), possibly created by reduction of iron at high temperatures in the presence of the assumed reducing carbon. It is thus concluded that only the resulting structures are influenced by the substrates and no significant differences in the magnetic performance of the resulting structures is noted.

As a control study, the synthesis process was repeated without filling alumina balls in the stainless steel cell. CB, ferrocene and nickelocene were weighed in the ratio of 1:5:5 (0.1g: 0.5g: 0.5g), mixed well together with toluene, and ultrasonicated for 15 min. The mixture was transferred to an empty stainless steel cell. The furnace temperature and inert atmosphere conditions were same as in the previous experiment. This particular sample taken from stainless steel after cooling was named

CN3. In order to examine how the stainless steel surface as substrate influenced the structural properties of the nanostructures transformed from CB at low temperature (1000 °C) transformation, we characterized sample CN3.

TEM analysis (not shown here) reveals that the sample CN3 contains only concentric layers without any parallel stacking, almost similar to CB structure. Based upon the synthesis and experimental characterization, we thus conclude that the stainless steel surface, when used alone, is not an effective substrate for this kind of low

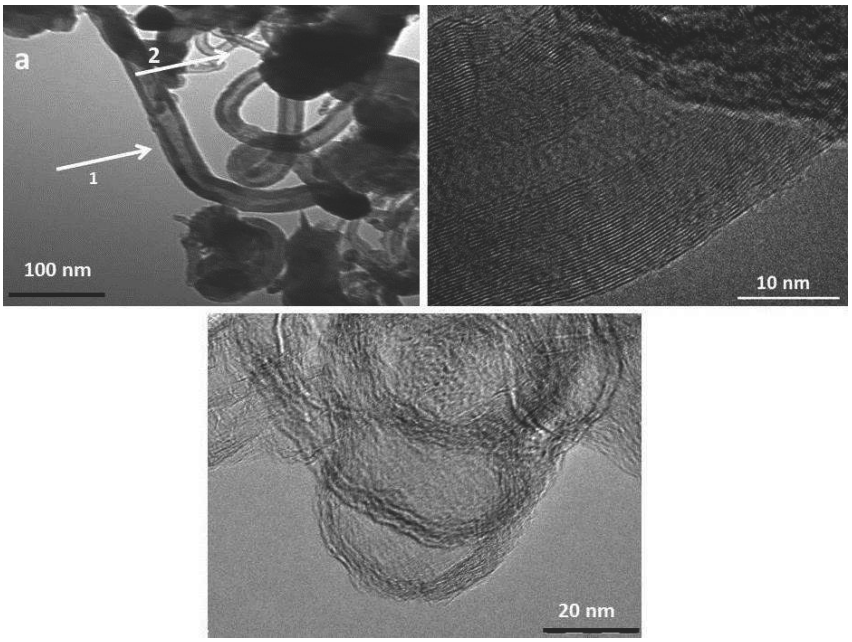

***Figure 5.2**: TEM (a) and HRTEM (b and c) images of CN2 nanotubes. Refer [131].*

temperature transformation of CB into nanotubes with the rate of annealing temperature of 10 °C/min. Our results is in accordance with the observation made by Donnet J.B. et al [46] who reported that the transformation of CB into nanotubes did not occur even when the rate of thermal annealing was 50 °C/min with stainless steel as substrate. As discussed in the analysis of CN2, nanotubes are obtained only when

alumina balls are used together with stainless steel in the presence of a bimetallic catalyst, Fe-Ni.

In order to study the dependence of successful transformations of CBs to CNTs on the weight ratios of CBs and metal catalysts at low synthesis temperature of 1000 °C with low heating rates of 10 °C/min. CB, ferrocene and nickelocene were weighed in the ratio of 1:1:1 in this experiment. The sample CN4 was collected after transformation with alumina balls in a stainless steel cell as substrate and sample CN5 was collected from the stainless steel surface after transformation.

TEM, HRTEM, XRD and Raman analysis of samples CN4 and CN5 showed no signs of graphitic transformation. The transformation of CB in such processes occurs only with certain critical ratio of weights of CB and metals [22]. There can be two reasons for this: lower metal density with respect to carbon species in the reaction vessel can make it difficult for the metal nanoparticles to consume the high content of carbon to form graphene layers on it or higher carbon density compared to organometallic compounds can poison the reaction and restricts the metal nanoparticles to be formed. The above results of CN4-CN5 indicate that the transformation of CB into nanotubes is not only strongly dependent on the substrate but also on the weight ratio of CB to ferrocene: nickelocene. By using different weight ratios of CB and the organometallic precursors, our studies showed that the optimum weight ratio of CB: ferrocene: nickelocene had to be 1:5:5 for successful transformation of CB to CNTs with alumina as substrate at low synthesis temperature of 1000°C and at low heating rates of 10°C/min.

5.1.3 Effect of Temperature:

In this section, research work carried out for paper III is explained [136]. The experiments were carried out at 700 °C and 1000 ºC with the samples taken in ceramic boat. The weight ratio of CB to ferrocene for these experiments was 1:10. The samples are named CNT700 and CNT1000, respectively.

SEM, TEM and HRTEM images are depicted in paper II. An increase in the synthesis temperature from 700 ºC to 1000 ºC influences the morphology of the produced nanotubes considerably. The nanotubes in the sample produced at 1000ºC contained different morphologies compared to the nanostructures in the sample produced at 700 ºC. The sample produced at 700 ºC contains only nanotubes but the sample produced at 1000 ºC was observed to contain both nanotubes and metal-encapsulated onion like nanostructures. The length of the nanotubes are almost uniform in the CNT700 sample while both long, (narrow and straight) nanotubes and short (bent and twisted) nanotubes are observed in the sample produced at 1000 ºC along with smaller nanotubes grown from the sidewall of the longer tubes.

The interlayer spacing measured using HRTEM analysis in the samples CNT700 and CNT1000 is almost similar at some regions (3.5Å). There are also some regions within CNT1000 where the interlayer spacing is measured to be around 3.45 Å. The HRTEM analysis in paper III [136] shows that the quality of nanotubes synthesized at both the temperatures are equal, even though there is a slight variation in the measurements. However, in depth analysis shows different phenomena. For example, from the figures 2c and 5b in our research work [136], one can note that the CNT700 sample contains nanotubes with walls not aligned parallel to each other while CNT1000 contains walls almost straight and aligned parallel to the tube axis.

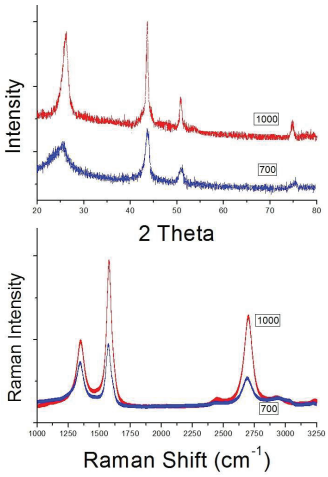

***Figure 5.3**: (a) XRD peaks and (b) Raman spectra of nanotubes synthesized at 700 °C (blue) and 1000 °C (red).*

Raman analysis and XRD measurements *(figure 5.3)* further show that the sample CNT1000 contains nanotubes of higher degree of crystallinity than the nanotubes of CNT700. The values of (ID/IG) calculated from Raman spectra in *Figure*

5.3 for the samples CNT700 and CNT1000 are 0.78 and 0.50 respectively. Low ID/IG values are assumed to denote well-graphitized CNT. Low ID/IG values are assumed to denote well-graphitized CNT. From these values, CNT1000 has a higher degree of graphitization than CNT700.

From the XRD measurements it is clear that both the samples contain peaks at $2\theta \approx 26°$ and 43.6°. The first one corresponds to the (002) planes of graphitic structures and the second peak corresponds to (100) planes of graphitic structure [22, 137], and both of these peaks can be treated as validation of the successful transformation of CB to graphitic nanostructures. The narrower peak for CNT1000 indicates that its degree of graphitization is higher than for CNT700. The other two peaks at $2\theta \approx 51.0°$ and 75.0° in both the samples can be attributed to iron carbide [22].

The interlayer spacing d_{002} in CNT700 and CNT1000 is around 3.47 Å and 3.44 Å, respectively while the parental CB shows interlayer spacing d_{002} around 3.66 Å. The interlayer spacing of both the samples is found to match with the inter-planar distance in a graphitic structure (3.35Å) [138], which further shows that CNT1000 contains more graphitized structures than CNT700.

Successful structural transformation of carbon black (CB) into nanotubes is carried out in the presence of an organometallic compound (ferrocene) at low synthesis temperatures of 700 ºC and 1000 ºC for the first time and the influence of the temperature in the transformation process is studied. Our study confirms that at low synthesis temperatures and with the aid of an organometallic compound (ferrocene) as the precursor for the catalyst, good quality CNTs can be obtained from CBs through a simple synthesis process. An increase in the synthesis temperature from 700 ºC to 1000 ºC influences the morphology of the produced nanotubes considerably. The nanotubes in the sample produced at 1000 ºC contained different morphologies compared to the nanostructures in the sample produced at 700 ºC. Both long, narrow and straight nanotubes and short, bent and twisted nanotubes were observed in the sample produced at 1000 ºC along with smaller nanotubes grown from the sidewall of the longer tubes. The sample produced at 700 ºC contains only

nanotubes but the sample produced at 1000 ºC was observed to contain both nanotubes and metal-encapsulated onion like nanostructures. Further characteristic studies are needed to study the magnetic and optical properties of the samples to evaluate the quality of these samples and to find possible applications.

5.1.4 Effect of carbon to metal ratio in the transformation of CB:

The paper IV [139] discusses the effect of the carbon to metal weight ratio in the transformation studies on CB into graphitized nanostructures. The experiments were conducted at 1000 ºC and all other parameters were unchanged. Ferrocene, nickelocene and CB were used in the prescribed weight ratio presented in the following table. CN1, CN2, CN3, CN4, CN5 in paper IV are referred to as F5N5, F5N2, F2N5, F10 and F2N2, respectively, and the notation F and N is referring ferrocene and nickelocene.

The I_D/I_G values listed in Table 1 [139] indicates that the F5N5 and F10 samples have a higher degree of long range crystal order than the structures in samples F5N2, F2N5 and F2N2 and the sample F2N2 has a lower degree of crystal order than the other four samples.

From the XRD measurements, the interlayer spacing d_{002} obtained for F5N5, F5N2, F2N5, F10 and F2N2 are found to be around 3.41 Å, 3.44 Å, 3.47 Å, 3.44 Å, and 3.44 Å respectively while the parental CB shows an interlayer spacing d_{002} around 3.66 Å. The interlayer spacing of all the five samples are found to match well with the inter-planar distance in a graphitic structure (3.35Å) [138]. As similar to the interlayer spacing $d_{002,}$ the crystallite size, L_c, values listed in table 1 indicates that the samples F5N5 and F10 contains higher degree of graphitized products than the other samples. The degree of crystallinity trends are F5N5>F10>F5N2 >F2N2>F2N5>Timcal 350G.

When comparing the samples F5N5, F5N2 and F2N5, it is clear that the small variations in the catalyst composition result in wide morphological variations. In addition, notable variations in crystallinity of F5N5, F5N2 and F2N5 samples are also

***Table 5.2**: Summary showing the CB to catalyst weight percentage and their impact on the transformation process analyzed using XRD, Raman, TEM, and HRTEM. Reference [139].*

Sample Name	*CB:F:N (wgt ratio)*	*XRD Lc (Å)*	*Raman I_D/I_G*	*TEM d_{002} (Å)*	*XRD d_{002} (Å)*	*Diameter (nm)*	*Resulting structure and description*
F5N5	1:5:5	77.32	0.51	3.41	3.41	20-150	Multi-walled carbon nanotubes
F5N2	1:5:2	69.62	0.80	3.45	3.44	< 50	Multi-walled carbon nanotubes
F2N5	1:2:5	37.33	0.85	3.48	3.47	10-100	Multi-walled carbon nanotubes
F10	1:10:0	71.93	0.52	3.44	3.44	10-50	Multi-walled carbon nanotubes
F2N2	1:2:2	55.58	1.41	3.44	3.44		Multi-walled carbon nanobeads
Timcal 350G		21.84	1.14		3.66		

found from XRD results and HRTEM images. According to Qian et al. [83], the growth rate of nanotubes on nickel is higher than on iron since the activity of nickel is considerably higher than the activity of iron.

There is always competition between the two catalyst particles and this change the growth conditions even for slight variations in the composition. In addition, slight variation in composition of the catalyst also influences the carbon solubility into the catalyst system. This in turn influences the growth rate since the activation energy of the system is highly dependent on the composition of the catalytic compounds [85].

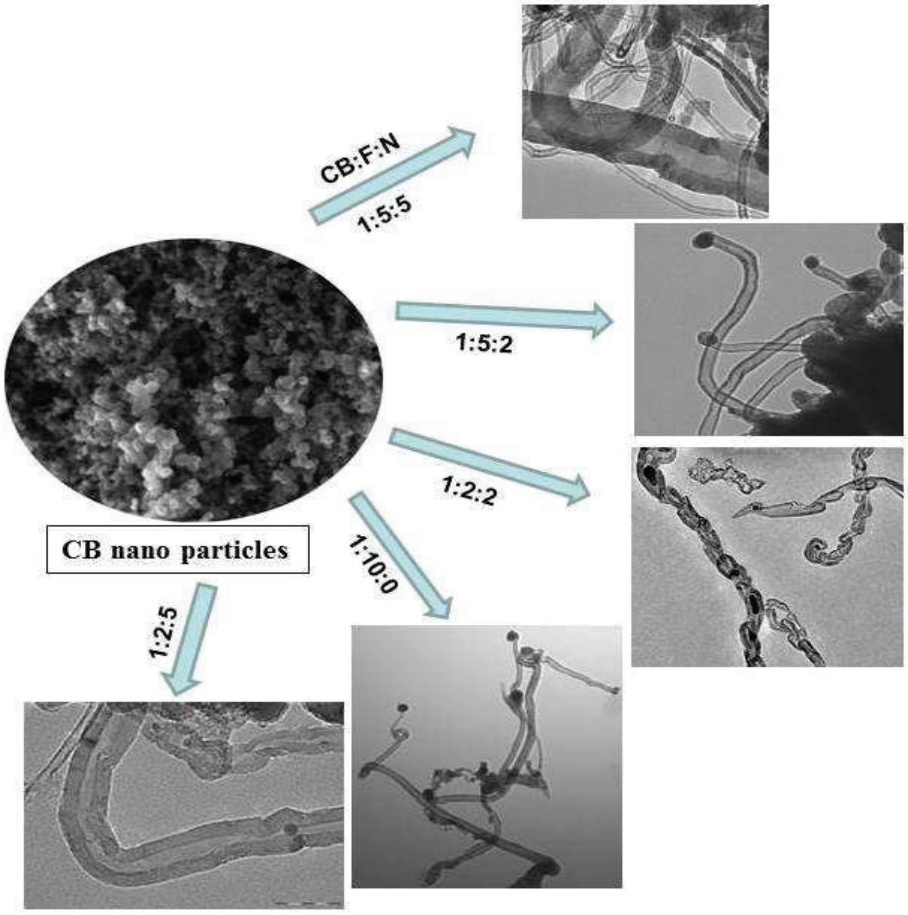

Figure 5.4: *Summary of TEM images obtained using different CB to catalyst weight ratio.*

F5N5, that has higher Fe-Ni content than F5N2 and F2N5, provides an energetically more favorable condition in the graphitization process and have high activation energy in the transformation process [75, 85]. Hence, F5N5 resulted in higher crystalline order structure than the other two samples.

As discussed by Rodriguez et al. [140], Fe:Ni alloys with higher iron content were found to show a higher activity in the nanotube growth in comparison with the case where the Fe:Ni ratio was equal or with the case where Ni content is higher and F5N2

is expected to have higher crystalline order than F5N5 and F2N5. In the present paper, results obtained were not in line with the above mentioned phenomenon. Chiang et al. [81] reported that the carbon solubility in Fe is slightly higher than in Ni and hence the possibility of formation of multi-walled tubes is higher in Fe rich systems than in Ni rich systems.

F5N5 and F5N2 samples with high Fe content does not seem to have notable variations in terms of tube walls.

As already mentioned above [74, 79, 80] and as expected, Fe-Ni catalyst show higher graphitization compared to mono-metallic catalyst, in particularly pure Fe catalyst, and matches the results discussed in paper IV that the F5N5 sample contains higher graphitized nanocarbon products than F10. However, the growth and morphological determination with respect to the catalyst variation needs to be studied.

The growth mechanisms of nanotubes via metal assisted synthesis are explained elsewhere [141-145]. The diffusion of carbon through the metal particle as well as segregation of the diffused layers in the form of ordered graphene layers have been suggested as key processes in the growth mechanism of carbon filaments and nanotubes [75].

5.1.5 Multi-walled carbon nanobeads (MWCNB):

The F2N2 sample obtained in our experiment is highly different from the other four samples. TEM images show typical nanobeads and metal encapsulated carbon nanostructures. Nanobead structures in long chains were found throughout the sample. This gives evidence for the high degree of transformation of amorphous carbon nanoparticles into bead-like structures.

The nanobeads obtained here are in long chain-like structures and can be described as one nanotube divided into small compartments as in bamboo-like nanotube structures [146, 147] and extended with many small beads. Beads are found with and without

metal particles, and the metal-filled carbon nanostructures are arranged in an irregular manner. It is not straight forward to suggest a growth model based on generally described tip and base growth modes [142, 148, 149].

The HRTEM images of individual metal-filled carbon nanobeads and metal-encapsulated carbon nanostructures are shown in figure 5.5 in this thesis. Figure 5.5a Typical TEM image of F2N2 sample of metal-encapsulated multi-walled nanobeads

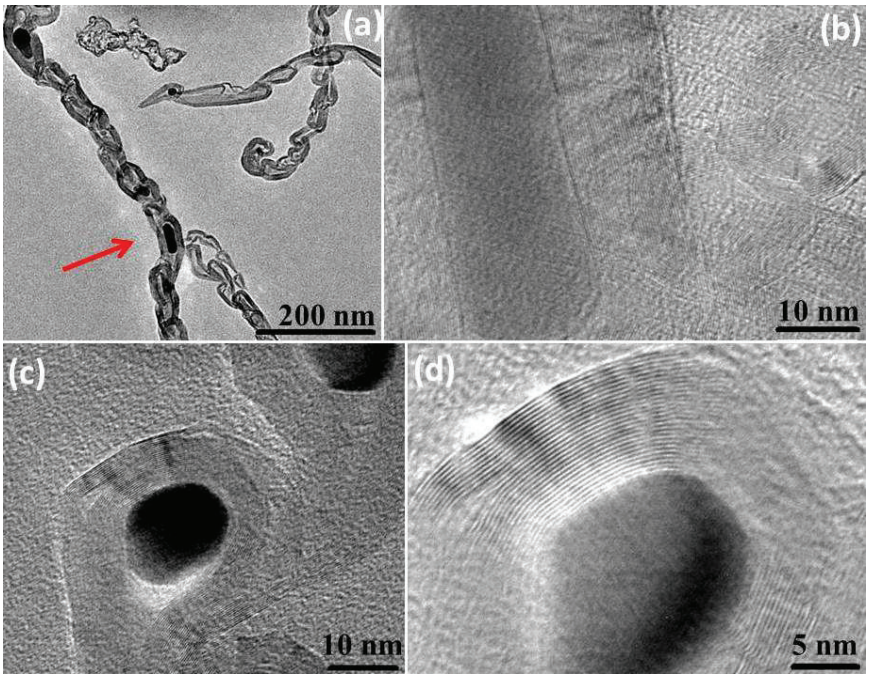

***Figure 5.5**: (a) HRTEM images of F2N2 sample displaying typical image of MWCNB, (b) displaying the closer look of single metal-encapsulated MWCNB, (c) shows a metal-encapsulated onion-like structure and (d) closer look of onion-like structure showed in (c). Reference [139].*

structures (MWCNB) is displayed in figure 5.5a and magnified portion of MWCNB in figure 5.5(a) showing a long chain-like structure (indicated by the arrow) is shown in figure 5.5 b.

These images confirm the presence of highly crystalline layers of carbon nanobeads and metal-filled carbon nanostructures. From HRTEM analysis, it is also clear that not all beads were filled with metal; in fact most of the beads are empty and hollow. The sample F2N2 also contains few metal-encapsulated carbon nanostructures and these are formed in a variety of shapes and sizes such as a rod-like structure, spherical structures and partly elongated structures with spherical head.

The inter-wall spacing in the metal-encapsulated carbon nanostructure is measured to be about 0.34 nm, closely matching with the inter-wall spacing of graphite [138]. Graphene layers are clearly distinguishable in both the bead structures and the onion-like structures, indicating a high crystalline nature of the sample.

As a whole, nanobeads were obtained with high quality and equidistant graphene walls. Compared to other the four samples, F2N2 is obtained with the lower amount of precursor.

The growth mechanism of the metal-encapsulated beads may be connected with the coalescence and deformation of onion-like nanostructures as similar to the mechanism explained by Kang et al. [145]. With slight variation of the catalyst weight ratio, F2N2 shows completely different morphological nanostructures compared to other four samples (F5N5, F5N2, F2N5 and F10). It is not straight forward to explain the difference in growth mechanism based on the catalyst variation alone.

The metal particles found in the sample F2N2 are around 10 nm in diameter. Small sized metal particles ($\leq$ 10 nm) are usually more catalytically active [14, 145] in the synthesis of graphitized carbon nanostructures and with the diffusion of carbon they become easily supersaturated and get fluidized well below their melting point. Finally, the carbon atoms precipitate more easily around the surface of a nanoparticle catalyst [14, 145, 150, 151]. The fluid-like nature of the metal leads to their easy encapsulation with graphitic layer formation. This is a possible reason for the formation of encapsulated metal nanostructures. Since the carbon shells can act as a

barrier against oxidation of metal nanoparticles, these metal-encapsulated carbon nanostructures can be used in high-temperature magnetic applications [14].

Similar metal-encapsulated multi walled carbon nanobead (MWCNB) structures have been reported in the work by Leela et al. [14] using methane decomposition over alloy catalysts (rare earth metal-transition metal based alloy) and have also been observed in the work of Kang et al [145] synthesized from the decomposition of methane by a CVD process using a Ni/Y catalyst supported on copper powder. However, in our present work, metal-encapsulated carbon nanobeads were obtained in a simple and single step process and with high degree of graphitization without any complicated steps in catalyst preparation.

The paper IV is concluded with following outcomes: Successful transformation of carbon black (CB) into carbon nano-beads and nanotubes was carried out using organometallic compound(s) as catalyst precursor(s) in a simple and single step CVD process. The catalyst precursor's weight ratio played a major role in determining the morphology of the graphitic products. Nano-onion like structures and metal-filled carbon nanotubes were obtained in vast quantity where the ferrocene content was high. In one of our experiments discussed in the present paper, we obtained metal-encapsulated nanobeads structures in a simple and single step process. The results also show that the use of bimetallic catalysts provide much different morphology and higher order crystal degree of carbon nanostructures than the use of mono-metallic catalysts.

5.1.6 Comparison on the effects of platinum and iron catalysts:

In this section, research works carried out for paper V [152] is discussed. The experiments were carried out at 700 °C with the samples prepared in a ceramic boat.

This study investigates the potential for Pt as a catalyst for solid-state structural transformation of CB. To the best of our knowledge, Pt has not been used before as a catalyst for the transformation of CB into graphitized nanocarbon. In addition, the role of iron-group metal in the transformation process was also been investigated.

We also intended to compare the results of the transformation process using a metal catalyst with high carbon solubility and a high carbon diffusion rate with a metal catalyst with low carbon diffusion rate. Hence, ferrocene, which can generate nano-sized iron particles, was chosen. These nanoparticles may then act as catalysts. Other researchers have also used ferrocene for the synthesis of carbon nanotubes [153-155].

In this work, H_2PtCl_6 was used as a source of Pt catalyst, with vitamin B_2 as a reducing agent. The basic principle of preparing such noble metal catalyst

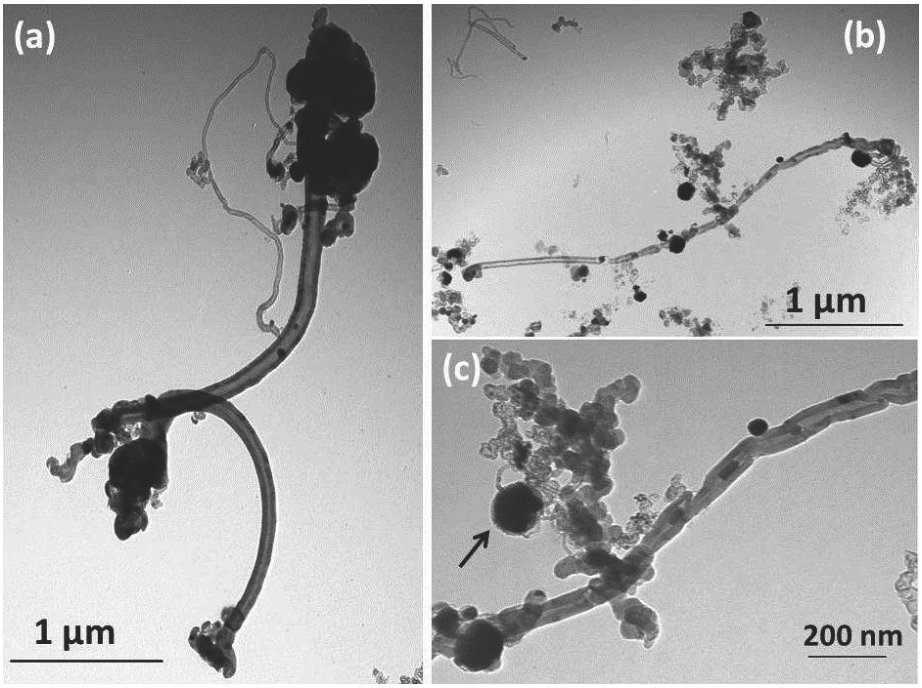

***Figure 5.6**: (a), (b) and (c) TEM images of CNPt sample: (a) nanotubes up to 2-3 µm in length with diameters that vary from 20 nm to 150 nm, (b) a long nanotube structure with a number of catalytic nanoparticles/nanorods filled inside nanotube (c) magnification of the right part of (b). The arrow in (c) shows large-sized metal nanoparticles encapsulated by a few layers of carbon. Reference [152].*

nanoparticles was adapted from the work of Mallikarjuna et al. [156].

In the first experiment, 10 ml of H_2PtCl_6, 50 mg of vitamin B_2 and 15 ml of isopropanol were mixed together and placed in a glass beaker of 100ml. The mixture was hand-shaken and heated in a water bath for 2 hours at 80 °C using a hot plate. The beaker was then removed from the water bath and heated directly on the hot plate at 200 °C for 1 hour. Afterwards it was washed with distilled water several times and heated at 120 °C for 12 hours. Later, 50 mg of CB (Timcal Ensaco 350G) and 15 ml of toluene were added and mixed together. Finally the mixture was ultrasonicated for 15 min and loaded into a ceramic boat and the experiment was conducted at 700 °C. The sample is named CNPt.

In the second and third experiments Timcal 350G and XC72R were used. CB and ferrocene were taken at a weight ratio of 1:10 and mixed with toluene and were subjected to ultrasonic vibration and the mixture was transferred to a ceramic boat. The experiments were conducted at 700 °C. The samples are named CNT700 and CNX700, respectively. The letter 'T' and 'X' denotes directly to the CB, Timcal 350G and XC72R, respectively. In the paper V [152], these samples are referred as CNT and CNX, respectively. The figures 5.6-5.9 are displayed below to get an overview of the samples CNPt, CNT700, CNX700 and CNG.

TEM images of CNPt (f*igure 5.6*) shows nanotubes up to 2-3 µm in length with diameters that vary from 20 nm to 150 nm (*figure 5.6a*). CNPt also contains a long nanotube structure with a number of catalytic nanoparticles/nanorods filled inside the nanotube throughout its length at irregular intervals (*figure 5.6b*). It can also be noted that the nano-sized platinum particles are present both inside and outside the nanotubes.

In addition to the normal nanotubes which are of single unit, the CNPt sample also contains few nanotubes whose tubular axis is not straight but continuous; instead it contains many compartments which are either filled with metal nanoparticles/nanorods or hollow and which have a wide variation of diameters. It may be united from many of the nearest small nano-units, which encapsulated the

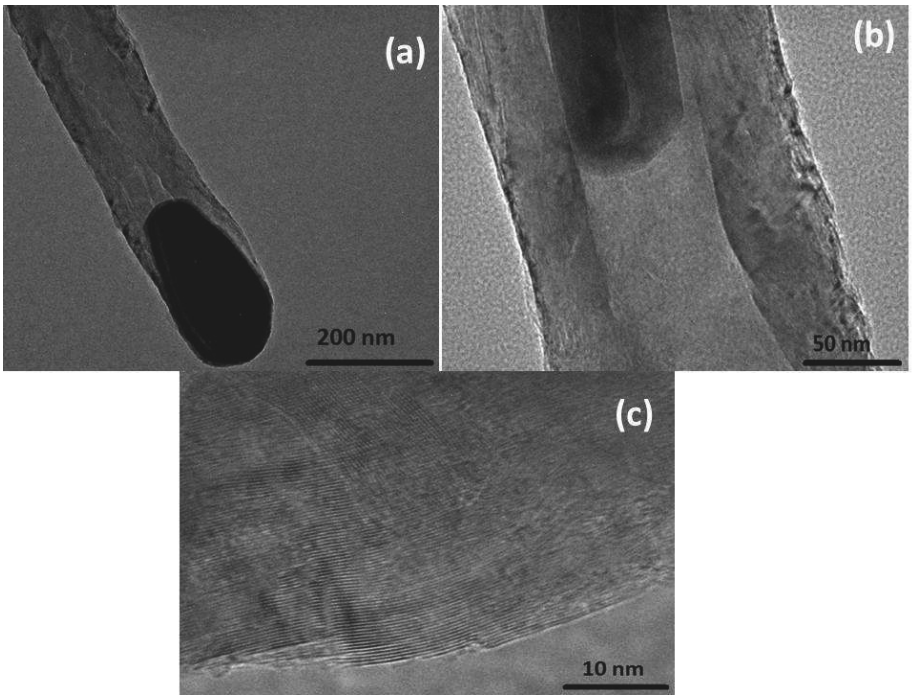

***Figure 5.7**: HRTEM images of CNT700: (a) one end of nanotube with a clearly visible metal nanoparticle, (b) nanotube which contains an internally grown metal-filled nanotube structure of diameter 50 nm; (c) a closer look at graphene layers in one of the nanotubes. Refer [152].*

metal nanoparticle. The metal catalysts encapsulated within a tube are in both spherical and elongated forms and these catalytic particles within a tube may not be formed from the fragmentation of large particles. Instead, we suspect that two metal nanoparticles at the nearest juncture encapsulated by onion-like structure may have coalesced together and extended as the tube, similarly to the mechanism proposed by Khang et al. [145].

This theory may be supported by the fact that, due to their high curvature, the fullerenes and onion-like carbon nanostructures possess high surface tension and high thermal reactivity. In order to reduce their surface energy and become thermodynamically stable, these structures tend to coalesce under suitable conditions

to form extended structures [157, 158]. Experiments on induced coalescence of C_{60} molecules in hot vapors carried out using mass spectrometry and fullerenes encapsulated in nanotubes [159-161] prove the possibilities of such coalescence of small carbon nano-spheres into a small compartment, which results in chain-like structures.

The CNT700 sample (refer (*figure 5.7*)) has nanotubes with metal fillings but not divided into many compartments and most of the tubes are grown with only slight

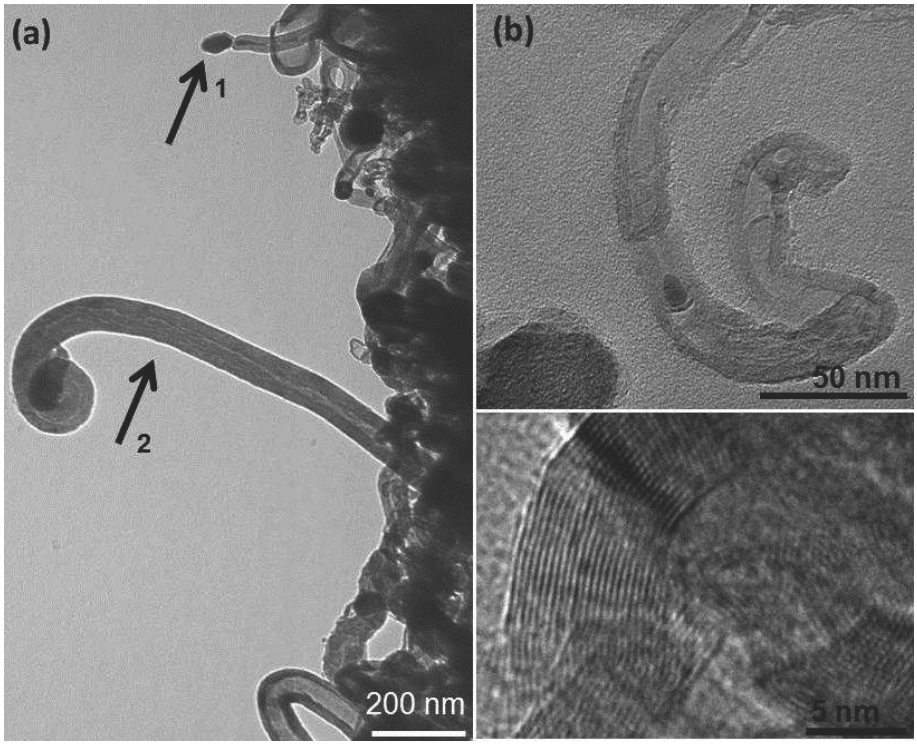

***Figure 5.8**: TEM images of CNX. The inset in (a) shows a closer view of the part pointed out by arrow 1. Arrow 2 shows a different nature of nanotubes with and without metal-fillings. (b) HRTEM images of CNX700 shows a nanotube, whose wall is divided into small compartments, (c) graphitic structure, which contains nearly 20 graphene layers. Refer [152].*

variation of diameters. Descriptions of which are already given in previous section. The CNPt sample has Pt nanoparticles formed around 20-150 nm and less, while CNT700 samples contains metal nanoparticles around and up to 300 nm. The former with large diameters (in this case around 80 nm and above), found encapsulated by onion-like structures, while the latter consists only of nanotubes with metal nanoparticles even up to 300 nm.

The TEM and HRTEM images show that CNT700 (*figure 5.7*) contains nanotubes with mostly distorted walls while CNX700 contain nanotubes with well-arranged graphene layers (f*igure 5.8*). CNT700 contains nanotube structures with a polycrystalline nature, and the sample CNPt contains amorphous carbon particles together with nanotubes.

All the three samples, CNPt, CNT700 and CNX700 contain encapsulated metal particles in the fcc phase. The CNPt contain particles in normal metallic form as platinum group metals (including Rh, Pd, Os, Ir, Pt) and do not form carbides at the present temperature range while the other two samples with Fe as catalyst, usually forms carbides [162]. The discussion above regarding formation of an fcc phase and carbides has already been verified by the XRD results. The CNPt sample shows XRD peaks related to only platinum nanoparticles while CNT700 and CNX700 shows XRD peaks related to iron carbides in addition to the peaks related to that of graphitic structures.

From XRD analysis, the interlayer spacing d_{002} in CNPt, CNT700 and CNX700 are found to be around 3.46 Å, 3.47 Å, and 3.44 Å, respectively, while the parental CB shows an interlayer spacing d_{002} around 3.66 Å [152]. The interlayer spacing of the samples CNPt, CNT700 and CNX700 is found to be closely related to the inter-planar distance in a graphitic structure (3.35Å) [138].

In Raman spectra obtained for carbon nanostructures, the intensity- or area-ratio of the D1- to G-peak varies inversely with the in-plane crystal domain size (L_a) of various graphitic materials [110, 114]. The values of (I_D/I_G) for the samples CNPt, CNT700 and CNX700 are 1.00, 0.75 and 0.50, respectively. From these values, it can

be concluded that CNX700 has a higher degree of graphitization than CNT700 and CNPt, as indicated also in the XRD analysis. In addition, the degree of graphitization is higher for CNT700 than for CNPt.

Comparing TEM and HRTEM images, it is clear that the degree of graphitization is higher in CNX700 compared to the other two samples. Further, the measured interlayer distance between two adjacent graphene layers is 0.35 nm and 0.33 nm for CNT700 and CNX700, respectively. The measured graphene layer distance in CNX700 (0.33 nm) is very close to the interlayer distance for perfect graphite, 0.335 nm [138]. These findings are in agreement with both I_D/I_G values from Raman spectra of these samples shown above and also with the XRD analysis of the peaks in figure 1 of paper V [152].

Metal-carbon interaction plays a crucial role in determining the quality and morphology of nanotube formation [163-165]. In a specific experiment undertaken in conditions similar to ours, only differing by the carbon precursor (as here in CNT700 and CNX700), it was shown that the thermal behavior of CB and the interaction of carbon with metal nanoparticles can be influenced by the specific surface area of CB [166, 167]. CBs produced in different processes (here Timcal 350G and Cabot XC72R) vary completely in their physical properties (including porosity, surface area, and particle size).

Due to their variation in the surface and structural properties, their surface reactivity, surface energy and the chemical reactivity differs from one CB product to another, even when they are treated in a similar experimental condition [168, 169]. This difference in their reactivity makes a reaction path including the interaction of metal catalyst and formation of graphene layers proceeds in a different way.

As previously stated [167] the surface area of XC72R and Timcal 350 G is 241 and 777 m^2/g respectively. We suspect that this variation might make a difference in the reactivity of the two CBs. However, this may vary when other conditions such as catalyst, temperature, or substrate changes. Even though there are studies that confirm that the surface properties and molecular structure of the carbon precursor determines

the quality and morphology of carbon nanostructures [170, 171], an atomistic approach of different CBs in the nanotube formation at the given experimental condition is yet to be studied.

In any reaction involving the transition metals and the carbon, d-orbitals of the metal tend to overlap with p-orbitals of the carbon, and hence the growth difference can be explained on the basis of electron vacancies in d-orbitals of metals, as recently proposed by Esconjauregui et al. [172]. These tendencies of overlapping d- and p-orbitals of metal and carbon, respectively, correspond to the metal-carbon reactivity and determine the carbon solubility limit in metal.

Compared to Pt as catalyst, Fe has higher d-orbital electron vacancies; hence carbon solubility in Fe is also higher, which in turn should correspond to the increase of reactivity where Fe catalysts are used. The interlayer spacing values determined in XRD and HRTEM analyses, confirm that the CNX700 sample has a higher degree of graphitized structures than CNPt. Nevertheless, the analysis of CNT700 does not lead to a similar conclusion. The degree of graphitization in CNPt is similar to the CNT700 samples as found in XRD and HRTEM analyses. This further shows that there must be other factors, influencing the reactivity path.

According to previous research (see for instance [132, 143, 173]), it is well known that the size of the catalyst also plays a crucial role in the determination of nanotube growth and its morphology. By comparing with the HRTEM images it is clear that both CNPt and CNT700 contain metal nanoparticles whose diameter varies significantly: 30-200 nm and 50-400 nm, respectively, while CNX700 contains nanotubes of diameter 50-100 nm.

5.1.7 Low temperature transformation studies:

Paper V further explores the possibilities of low temperature transformation mechanism. The experiment was conducted solely to emphasize the possibilities of low temperature transformation (around 400 °C) of CB into graphitized carbon

nanostructures and not for comparison with the other samples, since the reaction condition was essentially different.

In this experiment, the mixture containing CB (XC72R from Cabot Corporation), ferrocene and ethanol (50 mg, 0.5 g and 15 ml respectively) was subjected to ultrasonic vibration. The mixture was then transferred to a 200 ml glass beaker. The beaker was covered using a glass lid and subsequently heated on a hot plate at 400 °C in a nitrogen atmosphere for one hour. The temperature was measured using an IR thermometer focused at the center of the bottom of the beaker. Nitrogen gas was injected in atmospheric pressure into the beaker through a gap at the neck of the beaker using a long needle. The sample collected finally was named CNG.

HRTEM analysis (refer *figure 5.9*) showed that the sample CNG does not reveal any

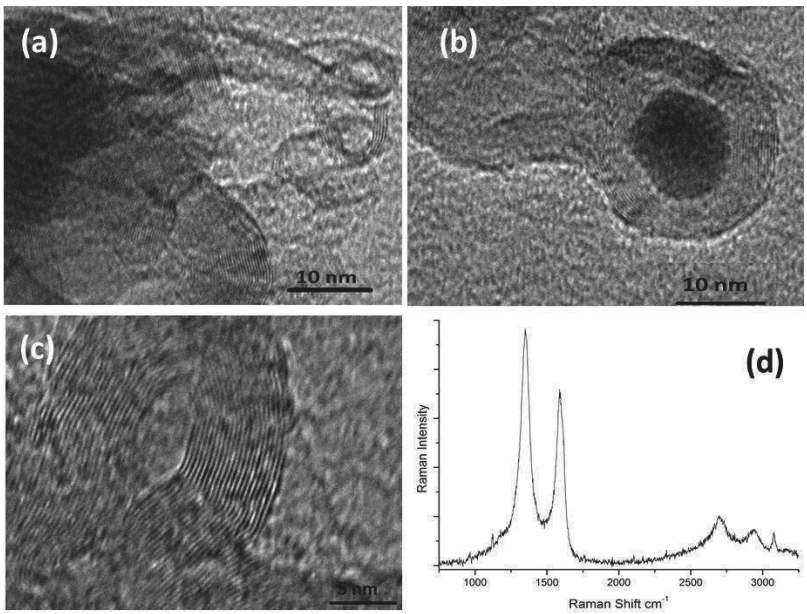

Figure 5.9*: (a-c) HRTEM images of CNG showing wire-like nano structure (a), metal-encapsulated onion-like nanostructure (b) closer view of the wire-like nanostructure in other regions of the sample and (c) Raman spectrum of CNG (d). Refer [152].*

nanotube structures and it has a different morphology than the three other samples discussed. HRTEM analysis showed that some part of the sample (right side of figure 5.9a) contains nanowire-like structures with nearly 5 graphene layers and few regions with metal-encapsulated onion-like structure that contains nearly 20 graphitic layers (*figure 5.9b*). Figure 5.7c shows a closer look at the curved nano-wire like structure, which contains nearly 20 graphene layers.

Since the glass beaker was purged with nitrogen gas slightly above atmospheric pressure, through a gap at the neck of the beaker using a long needle, there is a possibility for a slight pressure builds up in the glass beaker during the reaction, but as the system is not closed the increase in pressure is probably insignificant.

Effective low temperature decomposition of ferrocene is possible in an inert atmosphere [174]. Ferrocene itself can produce carbon during decomposition; moreover, the availability of an additional carbon source (in this experiment CB) can accelerate the reaction [175]. We propose that the above-mentioned parameters: the experiment conducted in an inert atmosphere with continuous flow of N_2 gas, and availability of carbon and metal precursor in the same phase enable a solid phase transformation at a very low temperature.

Reaction kinetics are possibly needed to bring more insight into the solid phase transformation process including the derivation of carbon from ferrocene and ethanol. However, no such effect has been considered in the present study. The possible formation mechanism of a graphitized nanostructure in the CNX sample can be proposed briefly as follows: Ferrocene decomposes to iron and hydrocarbon products, possibly with an aggregated form of Fe_3C nanoparticles or clusters. Carbon species accumulate on the surface of Fe/Fe_3C which results in encapsulation of a well-ordered graphitic structure. Finally, the catalytic function of the metal would be impeded once the carbon encapsulates it completely.

Further, the Raman spectrum of CNG shows increased intensity of the D band (*figure 5.9d*). An increase in the intensity of the D band is expected in short MWCNTs and in onion-like nanocarbon structures [176]. ID/IG is measured to be around 1.35. The

increase in the relative intensity of the disordered mode for CNG can be attributed to the increased number of structural defects and sp^3-hybridization. Structural defects are created by the introduction of pentagons within hexagonal blocks of graphene layers when they are deformed (due to curvature, distorted graphene walls, etc.) [177]. The second order Raman spectra at 2950 cm^{-1} and 3250 cm^{-1} are specific bands that appear only for disordered carbon and nanostructured carbons.

The effect of a Pt catalyst in the transformation process at a low temperature experiment, as similar to the sample CNG, needs to be studied. This study may bring insight into the solid phase transformation process of CB into graphitized nanostructures and prove helpful in comparing the role of different metal catalysts containing d-orbitals.

5.2 Transformation using Microwave irradiation

In the paper VI, the solid-state transformation behavior of carbon black (CB) nanoparticles after irradiated with microwave energy was studied with and without influence of a metal catalyst. The CB sample was exposed to microwave radiation at power of 900 watts from the oven and collected after 15 mins and after 30 mins and 45 mins of irradiation. The samples were characterized using X-ray diffraction (XRD) measurements, Raman spectroscopy, scanning electron microscopy (SEM), high-resolution transmission electron microscopy (HRTEM) and thermal-gravimetric analysis (TGA).

Heating the samples with the use of microwaves is efficient and energy saving due to rapid, and volumetric heating [178, 179]. In addition, technologically important novel materials have been developed so far which cannot be synthesized through conventional methods [179-182]. Considering these advantages, microwave-assisted solid phase transformation processes are studied in the present work.

5.2.1 Experiments:

The CB used in the following experiments was ENSACO 350G provided by Timcal Graphite & Carbon and hereafter referred as Timcal 350G. For each experiment, a small quantity of CB (few mg) was placed in a glass beaker of 200ml, toluene (few ml) was added and the mixture was heated on a hot plate. First the temperature was raised from room temperature to 120 °C and kept at the same temperature for 30 min. Next, the temperature was increased to 200°C at a rate of approximately 5 °C for each 15 minutes, and maintained at 200 °C for 30 mins. Then heating was continued to 300 °C at an average rate of 5°C/min and then the rate was increased to 20 °C/min until the temperature of 500 °C was reached. 500 °C was maintained for 6 hours and finally the sample was allowed to cool. Few quantity of the sample was collected for further characterization and named CT500. The carbon sample was then placed in a polished ceramic cup and exposed to microwave radiation at power of 900 watts from the oven. The microwave oven was set to run continuously but was stopped after 15 mins, after 30 mins and after 45 mins for sample collection. The collected samples were named CT500-1, CT500-2, and CT500-3, respectively. A similar experiment performed with the addition of ferrocene (few grams) to CB and toluene. For the ferrocene experiment a sample was collected only after 30 mins of continuous microwave irradiation and named CFT500.

5.2.2 Results and discussion:

Results from the characterizations discussed above shows that microwave irradiation induced CB nanoparticles to transforms into nano–balls and nano–stick like structures. While nanoballs of almost 300-500 nm diameter is visible in all the samples irrespective of microwave irradiation time, amorphous nano stick–like structures are visible only in the sample collected after 30 mins of microwave irradiation. CB irradiated together with a metal catalyst resulted in metal-encapsulated onion like structures with perfectly arranged graphene layers, while CB irradiated alone resulted in nano-sticks with amorphous structure.

More detailed discussions can be referred in Paper VI. Here are the excerpts from the discussions:

Nano–balls were found in all the samples CT500-1, CT500 -2 and CT500-3, collected after microwave irradiation for 15 mins, 30 mins and 45 mins, respectively. The HRTEM images of the sample CT500-2 are displayed in *figure 5.10 a-c*. The CT500-2 sample contains both carbon nano sticks and carbon nanoballs. Figure 5.10a shows that the sample contains carbon nano-sticks of length around 200-250 nm and width around 50nm. A closer look of the sticks is displayed in *figure5.10b*. The lattice fringes in the sticks are not flat but slightly curved and arranged in a wave-like pattern. In addition to the sticks, spherical particles of diameters around 50 nm are also visible. This structure is untransformed CB nanoparticles. *Figure 5.10c* shows the HRTEM images of carbon nanoballs which is of typical structures found in all three samples CT500-1, CT500-2, and CT500-3, irrespective of microwave irradiation time.

5.2.3 Nano-balls:

As the nano –balls were found in all the samples CT500-1, CT500 -2 and CT500-3, collected after microwave irradiation for 15 mins, 30 mins and 45 mins, respectively, two conclusions can be made from the ball-like structures in all the samples. First, ball-like nanostructures formed during the first 15 minutes (CT500-1) appear to be highly stable and exist without any high degree of transformation, even after 30 and 45 mins of irradiation. Only the untransformed part in CT500-1 might be transformed with further microwave irradiation. Second, due to irregular microwave energy distribution, nano ball-like structures might be created continuously from untransformed CB particles throughout the experiment.

5.2.4 Nano-sticks:

The particle size of Timcal 350G is around 30-50 nm in diameter. The diameter of curvature at both ends of the nano-sticks formed is also measured to be around 50

nm. This suggests that few CB particles may be “fused” together and formed a carbon nano-stick. Possibly 6-7 carbon nanoparticles have been involved in the formation of sticks.

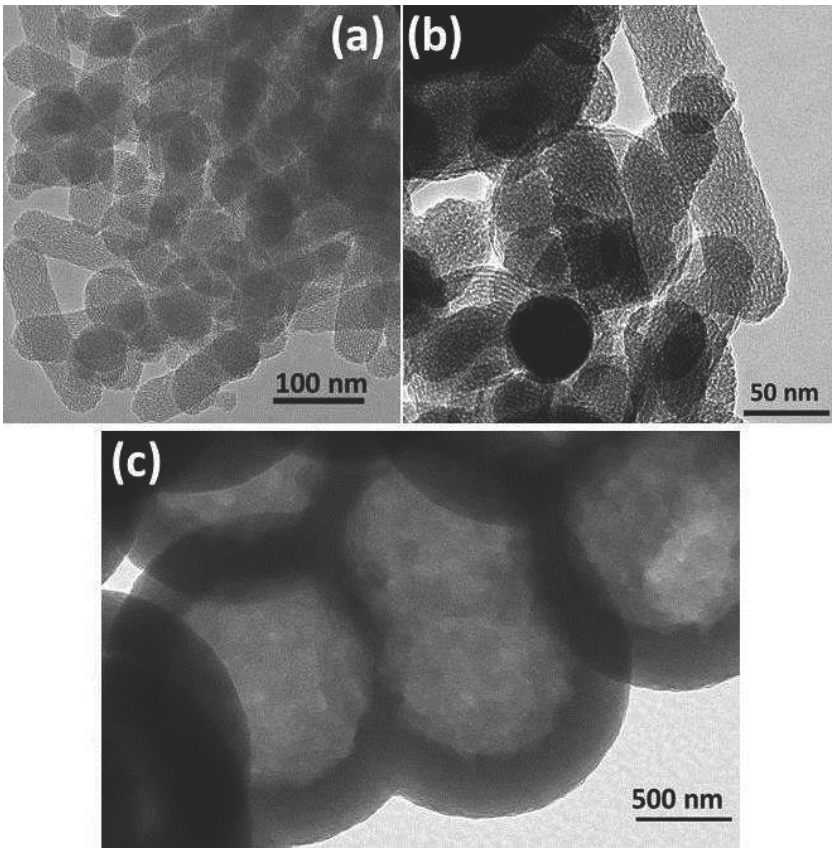

***Figure 5.10**: (a) HRTEM images of nanosticks found in CT500-2,(b) closer look of nanosticks and (c) HRTEM images of carbon nanoballs which is of typical structures found in all three samples CT500-1, CT500-2, and CT500-3.*

The experiments with microwave irradiation can be concluded as follows: The transformation of CB nanoparticles was carried out using microwave radiation and the influence of time and catalyst was performed with and without catalyst. Two different nanostructures were obtained via this process from CB nanoparticles of

diameter around 30-50 nm: nano-balls and nano-stick like structures. While nanoballs of almost 300-500 nm diameter is visible in all the samples irrespective of microwave irradiation time, amorphous nano-stick like structures are visible only in the sample collected after 30 mins of microwave irradiation. It is suspected that these two different structures were originated from two different structural orientations that CB has approached after reactions with toluene and microwave irradiation at the beginning. With iron nanoparticles present as catalyst, metal-encapsulated onion like structures with perfectly arranged graphene layers were obtained. It is also found that the transformation of CB particles occurred only after 30 mins of microwave irradiation.

5.3 Transformation experiments using closed quartz tube:

In this section, chemical vapor deposition (CVD) of multi-walled carbon nanotubes (MWCNTs) on nickel-coated sapphire substrate is reported here. The deposition of MWCNTs carried out at two different temperatures 700 °C and 850 °C is studied.

5.3.1 Experiments:

At first, a sapphire substrate was coated with nickel thin films of 16nm thickness via Balzers BAE 250 coating system. Next, sol was made by adding few ml of acetone to CB (Timcal Ensaco 350G) powder and then the mixture was subjected to ultrasonic vibration for 30 mins. Then the sol was poured into the quartz tube of length 80mm and diameter 6mm. Approximately, 15mm of bottom part of the tube was filled with carbon sol. A neck was formed at around 20-25 mm from the bottom of the quartz tube. Nickel thin films were kept at the middle of the quartz tube. Finally, the top end of the quartz tube was sealed and the tube was placed in a furnace. Two experiments were conducted with the similar steps mentioned above with two working temperatures. The samples were heated to 700/850 °C at a rate of 10 °C/min and kept

at 6 hours at the same temperature and then cooled at a rate of 5 °C/min. Samples were named CNF700 and CNF850 respectively.

5.3.2 Results and discussions:

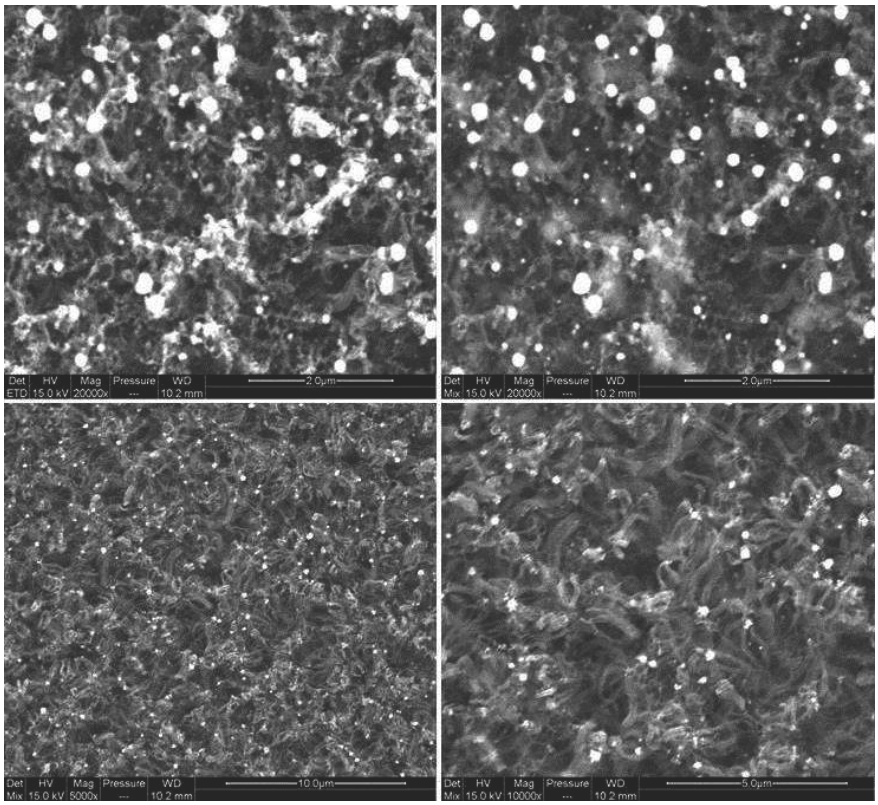

***Figure 5.11**: SEM images of (a-b) CNF700 and (c-d) CNF850.*

SEM images of CNF700 and CNF850 samples are shown in *figure 5.11(a-b) and (c-d)*, respectively. Many fibrous deposits were clearly observed on these sapphire substrates implying that the experiment achieved good yield.

At a first glance, it is also clear that the quality of nanotube formation is improved with increase in temperature. Both deposits contain Ni particles lifted out of substrates and now situation at the on top end of the nanotubes, which shows that the growth followed a tip-growth mechanism. The tubules are thick and short, and about 1-2µm in length in both deposits. There are no amorphous carbon deposits around the samples. Raman scattering spectra of Timcal 350G CB and the samples grown at 700°C and 850 °C are shown in a, b, c panels respectively in figure 5.12.

Figure 5.12 illustrates the Raman spectra for the CNF700, CNF800 and Timcal 350G. It shows that both the samples, CNF700 and CNF800, display notable

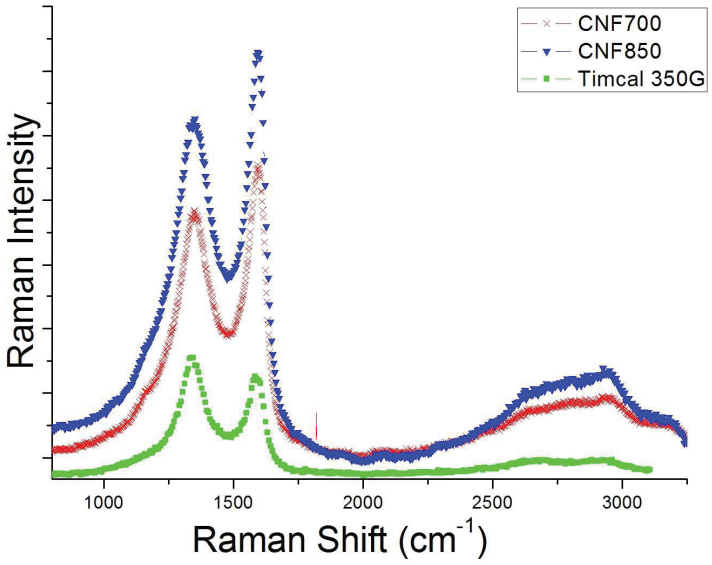

***Figure 5.12**: Raman spectra of (a) CNF 700 and (b) CNF850.*

variation at 1350 cm^{-1} (D1-peak) and 1580 cm^{-1} (G-peak).

The intensity- or area-ratio of the D1- to G-peak varies inversely with the in-plane crystal domain size (La) of various graphitic materials [110, 114]. In CNTs the ratio of the intensity of the D-line (ID) to the intensity of the G-line (IG), I_D/I_G increase

with increasing structural disorder, that is, I_D/I_G is regarded as a CNT morphology indicator. Low ID/IG values are assumed to denote well-graphitized CNT. The values of (ID/IG) for the samples Timcal 350G CB, CNF700 and CNF850 are 1.14, 0.84 and 0.85, respectively. ID/IG values holds for the proof for the graphitized structures available in CNF700 and CNF850 samples.

The present discussion about the transformation studies using CVD apparatus and closed quartz tube is to show yet another possible method of solid-phase transformation of CB into nanotubes. As far as now, it is clear that the temperature plays a major role in determining the morphology of the transformed products. The present experiment is still in preliminary phase. Further works are needed to elucidate the quality of the present work, including variation in metal coatings, film thickness, substrates and experimental temperature.

5.4 The chemical modifications reactions on CB

In this chapter, the results and discussions of the experiments related to the chemical modifications of CB is provided. CBs used in these experiments were Ensaco 350G provided by Timcal Graphite & Carbon and Vulcan XC72R provided by Cabot Corporation hereafter referred as Timcal 350G and XC72R.

5.4.1 The effect of solvents:

The results on the chemical modification of CB using di–carboxylic acids were already presented in Paper I. The excerpts of this paper are provided below:

We have presented a novel method for modifying the surface of CB using a simple heat treatment in the presence of a carboxylic acid and a solvent. CB was mixed with maleic acid and either water or ethylene glycol, and heated at 250 °C. Unlike the traditional surface modification processes which use heat treatment of carbon with mineral acids, the present modification method using a carboxylic acid proved to be

efficient, simple and fast. CBs from two different vendors were used, and the modified samples were characterized by TGA, BET surface area measurements, XRD, particle size and Zeta potential measurements, and FTIR. It was found that several material properties, among these the thermal stability and surface area, of the modified CB are significantly altered relative to the parental carbon samples.

Prior to the experiment, 1.0 g of CB was dried at 120 °C in an oven of compact air convection type to remove surface oxides. Afterwards, the dried sample was mixed with 1.0 g of maleic acid and 100 ml solvent. In the first experiment, where water was used as solvent, the mixture was subjected to ultrasonic vibration for 15 min to achieve complete dispersion of acid over the carbon samples. The mixture was then heated at 250 °C for 2 hours in the oven. This temperature was selected because it is well above the decomposition temperature of maleic acid (131-139 °C). The modified samples of CI and CII were named CI H and CII H, respectively.

In the second experiment, ethylene glycol was used as solvent and the mixture was stirred for 15 min using a magnetic stirrer and then heated at 250 °C for 3 hours in the oven. The time of heating was increased compared to the first experiment since the samples were not dry after 2 hours. The modified samples of CI and CII in this experiment were named CI G and CII G, respectively. Irrespective of the solvent used, the samples were all in pellet form after the heat treatment.

From table 5.3, the BET surface area of CI G and CII G is reduced by 90% compared to its respective parental carbon. A similar major reduction in surface area compared to the parental sample was reported for the reaction of CB with 0.1N H_3PO_4 [183]. Variations in surface area may be due to microstructure evolution after treatment with maleic acid in glycol. CB is a meso- and macro-porous material, and it also contains a small amount of micro-pores [21]. We may suspect that the reaction of maleic acid and glycol with CB strongly blocked the surface pores due to bulky compounds that formed during the reactions. For the case where water was used as solvent, this effect was much lower. The change in surface area gives clear evidence that treatment of maleic acid altered the carbon surface structure.

The average particle size of modified carbon is significantly smaller compared to the parental carbon, as listed in *table 5.3*. The reduction in size is between 51% and 77% for all samples. Whether the acidic treatment alone is responsible for this effect, or whether the ultrasonification in a solvent also influences the particle size by breaking down CB aggregates, cannot be determined from these experiments.

The zeta potential values (*table 5.3*) of all modified CB samples have more negative charges than the parental carbon, which means that the modified carbon black forms a more stable dispersion system than does the parental carbon [11, 184]. The charge reversal in the zeta potential value for CII H and CII G compared to CII, from positive to negative values indicates that the maleic acid modification provides similar surface groups on the two sample sets but with possibly different volume ratio.

With the reference to the TG graphs illustrated in *figure 1-2* of the paper I [167], the

***Table 5.3**: Surface area (BET), particle size and zeta potential measurements of parental and chemically modified carbon samples.*

Samples name	*BET S.A. (m^2/g)*	*Size measurement (d-nm)*	*Zeta potential (m/V)*
CI	*241*	*1309*	*-6*
CI H	*202*	*343*	*-21*
CI G	*20*	*298*	*-13*
CII	*777*	*1125*	*+2*
CII H	*700*	*553*	*-27*
CII G	*74*	*322*	*-10*

following remarks can be made: The chemical modification with maleic acid in water increases the thermal stability of the CB sample (only for CI and not for CII. CIIH shows slightly decrease in thermal stability compared to CII), while using ethylene glycol as solvent significantly decreases the thermal stability in both CI and CII samples. However, from the comparison of the thermal stability of modified samples using different solvents, it is clear that the chemical modification with maleic acid in water shows higher thermal stability than the use of ethylene glycol as solvent.

The following can be concluded from the above results. The reaction was carried out with two different solvents, and the reactions using water as solvent produced thermally more stable products compared to reactions using ethylene glycol. XRD confirms a slight increase in crystallinity for the water-modified samples and a significant decrease for the samples modified by ethylene glycol. From BET measurements, all samples have less pore surface area than the parental carbon, particularly CI G and CII G, and one may anticipate that surface groups block the pores. The zeta potential of all modified samples are shifted to more negative values, indicating better dispersion properties as a result of surface modification. In summary, the change in properties listed above gives clear evidence of the successful surface functionalization of carbon blacks with maleic acid.

FTIR spectra were recorded for the carbon samples, and the results for CI H and CI G, as well as for the parental carbon, are shown in *figure 5.13*. Even though CB is difficult to characterize using FTIR, analysis was done to possibly identify any surface groups that might be created after chemical modification. The CI H spectrum displays bands at wave numbers 1700-1300 cm^{-1} that indicate the presence of carbonyl or carboxyl groups [12, 96, 185]. In addition the spectrum shows strong bands around 1460-1420 cm^{-1} for CI H. These bands are often attributed to the OH in-plane deformation mode of the hydroxyl part of a carboxyl group. In addition, there are no strong peaks above 3000 cm^{-1} which would indicate hydroxyl groups in alcohols or phenols. This further confirms that these bands (1460-1420 cm^{-1}) most probably are due to carboxyl groups, stemming from the maleic acid.

The bands in the region around 1550 cm^{-1} may be due to C=C stretching vibrations in aromatic ring structures. The intensification of all these bands, compared to the parental CB, clearly shows the presence of functional groups on the surface. For CI G, we obtained FTIR spectra with only weak bands. Neither of the samples exhibited bands above 3000 cm^{-1}, thereby indicating the absence of alcohol functional groups.

For the second set of samples (CII H and CII G), we obtained similar spectra as for CI G. I.e., we did not succeed in obtaining any strong bands in the FTIR spectra of CII H and CII G. In our experience, reliable FTIR-spectra of CB are difficult, and sometimes impossible, to obtain. In light of this, for cases where IR shows clear, strong bands one may regard this as evidence for the presence of functional groups on

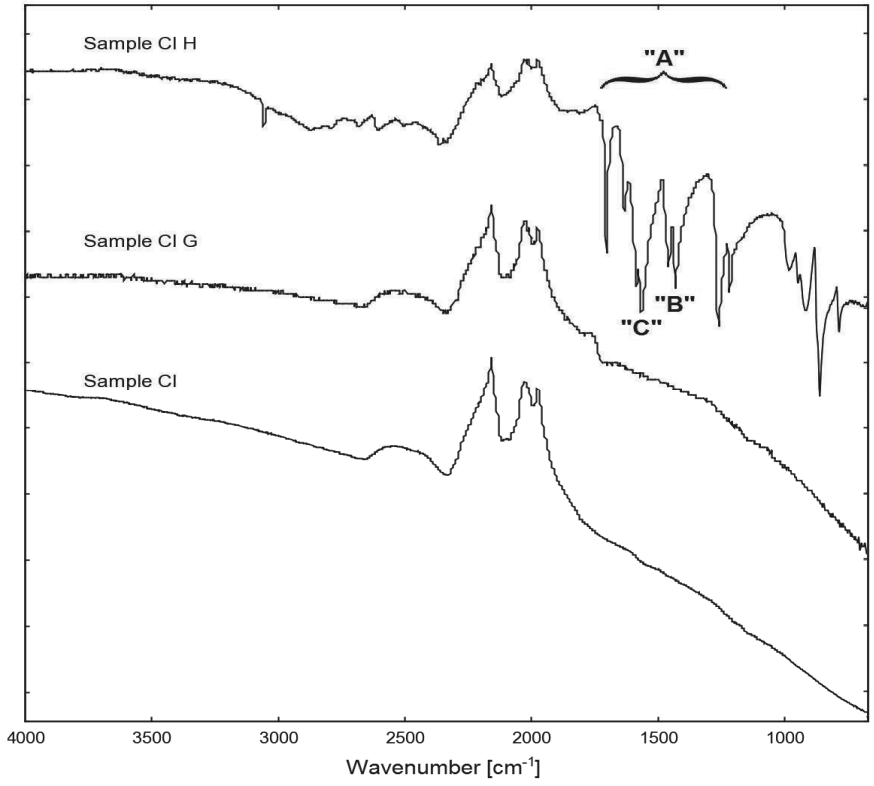

***Figure 5.13**: FTIR spectra of three samples: CI, CI G and CI H. Refer [167].*

the surface. On the contrary, a negative result from FTIR does not necessarily confirm the absence of functional groups.

5.4.2 The effect of pre-heat treatment on carbon black:

The reactions done in previous section discussed the effect of solvent in the chemical modification of CB using organic acid. In the following section, the reaction is performed to find out the effect of pre- heat treatment of CB samples on the reaction with maleic acid (di- carboxylic acid) and citric acid (tri- carboxylic acid). As both the maleic and citric acid varies with the concentration of hydroxyl and carboxyl molecules, surface reactions on the carbon is expected to be different.

In this experimental section, only minor works have been carried out and work should be extended in future to get more insight. A brief discussion with the help of TGA and BET surface area measurements has been given in this section. Further works needed in future to study the effect of functionalization in detail.

A CB samples, XC72R from Cabot Corporations and Ensaco 350G from Timcal Carbon and Graphite were purchased. Hereafter, the CB samples are referred as CI and CII, respectively.

The virgin samples of 0.1g were heat treated at 120 °C with and without inert (nitrogen) atmosphere. To compare the effect of pre-heat treatment on CB samples, the experiments were also done with as- purchased CB without any heat treatment.

Prior to the experiments, 0.1g of maleic acid (di- carboxylic acid)/ citric acid (tri- carboxylic acid) is added to CB and mixed with 10 ml of water. The mixture was subjected to ultrasonic vibration for 15 min to achieve complete dispersion of acid over the carbon samples. The mixture was then heated at 250 °C for 30 mins in the oven. This temperature was selected because it is well above the decomposition temperature of maleic acid (131-139 °C). Modified samples were characterized using TGA and BET surface area measurement techniques.

The summary of experiments and the BET specific surface area (BET SA) for parental and modified CBs are listed in table 5.4. BET specific surface area measurements shows that the samples treated with citric acid have shown lesser value than the samples treated with maleic acid.

Citric acid treatment would have possibly induced more functional groups than the maleic acid. With the increase number of intercalated molecules, the entry of adsorbing gas get blocked and hence the values of specific surface area in citric acid treated carbon samples is lesser. It can be concluded that the effect of functionalization on the carbon surface is more with citric acid treatment than with

Table 5.4*: Summary of the experimental details is given below. Here, CB, MA, CA refers to carbon black, maleic acid and citric acid, respectively. Except for the samples CM1, CC1, TM1 and TC1, all other samples were pre- heat treated at 120 ˚C in an oven with varying atmosphere (air or N_2).*

Sample name	Pre- heat treatment	CB (in g)	MA (in g)	CA (in g)	Temp. (˚C)	Time (mins)	BET SA *(m^2/g)*
CI							**241.67**
CM1	None	0.1	0.1		250	30	233.61
CM2	Air	0.1	0.1		250	30	183.74
CM3	N_2	0.1	0.1		250	30	220.18
CC1	None	0.1		0.1	250	30	97.24
CC2	Air	0.1		0.1	250	30	103.66
CC3	N_2	0.1		0.1	250	30	110.00
CII							**777.14**
TM1	None	0.1	0.1		250	30	690.27
TM2	Air	0.1	0.1		250	30	691.54
TM4	Air	0.1	0.2		250	30	725.31
TC1	None	0.1		0.1	250	30	531.56
TC2	In air	0.1		0.1	250	30	547.87
TC4	In air	0.1		0.2	250	30	572.92

maleic acid.

In the case of CI CB samples, there is slight differences noted in BET SA values of CM1 and CM3. However, the sample CM2 shows much lesser value of BET SA compared to other two samples, CM1 and CM3. It can be attributed to the fact that CM2 have more changes in their surface than other two samples. But in the case of CII (Timcal 350G), TM2 does not have notable difference in the value of BET SA compared to TM1, however, both these samples have much lesser BET SA values compared to the parental carbon. This indicates that irrespective of the pre- heat treatment process, surface of the CII sample have been modified by reactions with maleic acid.

Comparing the values of CC1, CC2 with TC1 and TC2, it can be easily noted that the difference in BET SA value is more between TC1 and TC2 than with CC1 and CC2. This shows that the reaction condition can also be influenced by the original pore structure and surface area of the parental carbon. Finally, it can be concluded that the reactions of citric acid have much influence in the surface properties of CB compared to maleic acid reactions, irrespective of the pre- heat treatment process on the CB.

There is also a notable variation in BET SA values with sligh increase in the quantity of maleic acid and citric acid taken during the reactions (TM2-TM4 and TC2-TC4). The increase in the quantity of organic acids can make huge difference in the surface properties of the carbon.

TGA graphs in *figure 5.14* shows that the maleic acid treated samples CM1, CM2, CM3 have higher thermal stability compared to the parental carbon, CI, irrespective of the pre- heat treatment process. Improved thermal stability in these samples indicates that the weak structures within the carbon samples are either removed or formed a stable structure after the reactions with maleic acid.

In contrary, CC1, CC2 have lesser thermal stability compared to the parental carbon CI. This can be related to the fact that these samples have more functional groups attached to the surface of the carbon. This is in accordance with the results of BET

SA. These molecules might be removed in the beginning of the thermal treatment before the whole carbon structures get collapsed. All the samples have shown complete burn out at around 700 °C irrespective of the initial weigh loss.

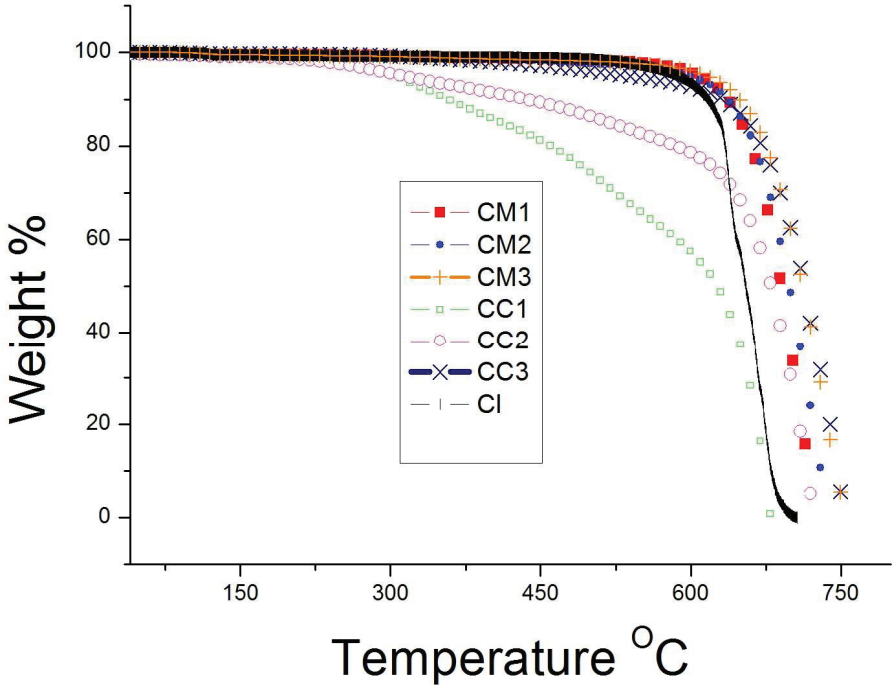

***Figure 5.14**: TG analysis of parental carbon CI and the modified samples.*

Out of other samples treated with citric acid, only the sample CC3, the sample pre-treated at N_2 atmosphere, shown higher thermal stability. There are possibilities for the surface functional groups attached to this sample as similar to CC1 and CC2, but possibly as more stable structures.

Figure 5.15 shows TG analysis graphs of parental carbon, CII and the modified samples TM1, TM2, TM4, TC1, TC2 and TC4. Here, both the citric acid and maleic acid modified samples display decrease in thermal stability with the parental carbon.

It is common for all the reactions irrespective of the variation of pre- heat treatment and organic acid quantities.

The conclusion can be drawn as follows: The pore size and surface area of the

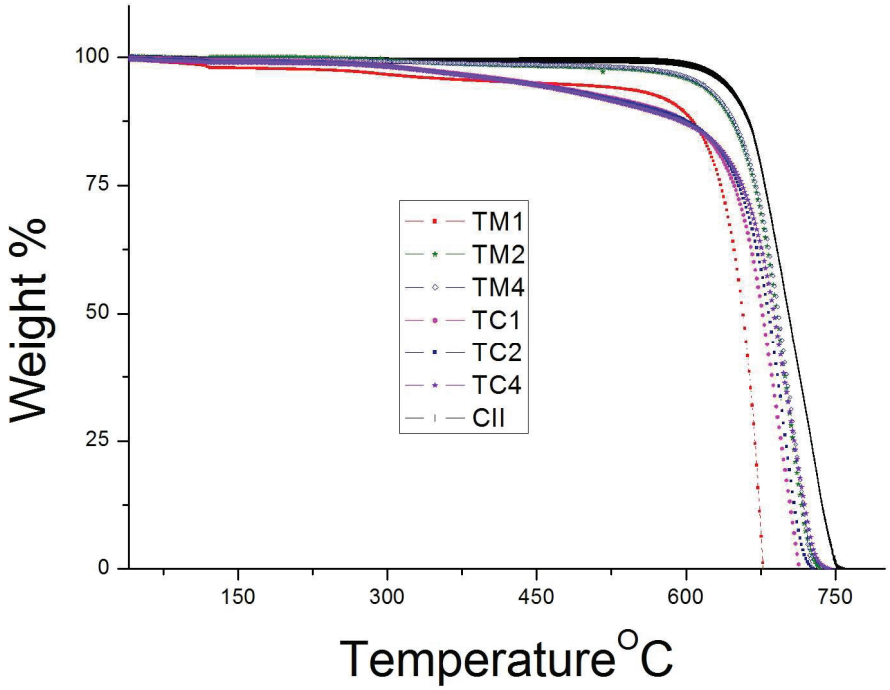

***Figure 5.15**: TG analysis of parental carbon CII and the modified samples.*

parental carbon plays a crucial role in the determination of the surface functionalization reaction with organic acids. The pre- heat treatment also have impact on the reaction conditions. However, these facts need to be verified in detail with more experiments and characterizations.

Chapter 6

Summary and future works

In the present project, the studies on the solid- phase transformation of CB into graphitized nano structures and the chemical modification of CB surface using carboxylic acids were performed.

In this work, an easy, economical and single-step solid- phase transformation studies, mono- and bi- metallic organic compounds as catalyst precursor and alumina boat as substrate was used. Change in parameters of temperature, inert gas, metal-catalyst ratio, mono- and bi- metallic catalysts, transition and non-transition metal catalyst, use of microwave energy irradiation with and without catalyst were studied. The products obtained in this work consists mostly of metal-encapsulated multi-walled carbon nanobeads (MWCNB), multi-walled carbon nanotubes (MWCNT), nano-balls and nano- onions.

The difference in mechanism of nanotube growth and the transformation of CB into graphitized nano-carbon related to different parameters mentioned above were discussed. Possible growth difference related to the catalysts, Fe and Pt, was explained on the basis of electron vacancies in d-orbitals of metals. It was also shown that the transformation of CB into graphitized nano structures can be carried out at a very low temperature (400°C).

In future, i) different catalyst with varying vacancies in d-orbitals will be used in the solid-phase transformation experiments and the effect on the transformation of CB into nanotubes will be explored, ii) different CBs with variation in the surface area and particle size need to be used in the transformation studies to explore the effect of physical properties of CB (XC72R from Cabot Corporations, Ensaco 350G and Ensaco 250G from Timcal Carbon and Graphite, and Conductive carbon from Pentacarbon), iii) variation of catalyst and preparation conditions are needed in the microwave experiment and finally iv) in the closed quartz tube experiment, thin film of different metals such as Fe, Fe-Ni, Pt, Ti of different thickness on the substrates of

SiO_2 and sapphire are planned to use to further study the process of transformation of CB on thin films with varying substrate conditions.

In the chemical modification studies on the surfaces of CB, di- carboxylic acid was used. Two solvents (water and ethylene glycol) are used in the reactions to study the change in effects in the surface modifications. It was found that several material properties, among these the thermal stability and surface area of the modified carbon black, are significantly altered relative to the parental carbon samples.

The experiments were conducted to study the following which need to be done in future: i) to study the influence of solvents as already done in the paper I [167], ii) to study the influence of di- and tri-carboxylic acids in the surface modification of CB, iii) to study the influence of pre-heat treatment with and without nitrogen atmosphere and finally iv) to study the effect of modified CB as a support for the electro-catalysts in the fuel cells (future works).

To get more insight into the chemical modification reactions, the experiments, with variation of solvents, organic acids and pre-heat treatment, will be extended to other commercial carbon black such as Ensaco 250G from Timcal Carbon and Graphite, Conductive carbon from Pentacarbon were purchased. The samples will be characterized using TGA, XRD, FTIR, Zeta potential measurements and BET studies.

Bibiliography

[1] Kreiter A, Czifra S, Bendő Z, Imre JE, Pánczél P, Váczi G. Shine like metal: an experimental approach to understand prehistoric graphite coated pottery technology. Journal of Archaeological Science. (0).
[2] Kwiecińska B, Petersen HI. Graphite, semi-graphite, natural coke, and natural char classification—ICCP system. International Journal of Coal Geology. 2004;57(2):99-116.
[3] Blank V, Popov M, Pivovarov G, Lvova N, Terentev S. Mechanical properties of different types of diamond. Diamond and Related Materials. 1999;8(8–9):1531-5.
[4] Brookes CA, Brookes EJ. Diamond in perspective: a review of mechanical properties of natural diamond. Diamond and Related Materials. 1991;1(1):13-7.
[5] Phillips D. William Lawrence Bragg. 31 March 1890-1 July 1971. Biographical Memoirs of Fellows of the Royal Society. 1979;25:74-143.
[6] Zhao J, Yang L, Li F, Yu R, Jin C. Structural evolution in the graphitization process of activated carbon by high-pressure sintering. Carbon. 2009;47(3):744-51.
[7] Zhang P, Tay BK, Sun CQ, Lau SP. Microstructure and mechanical properties of nanocomposite amorphous carbon films. Journal of Vacuum Science & Technology A. 2002;20(4):1390-4.
[8] Tessonnier J-P. Carbon Nanomaterials: Synthetic Approaches. Nanotechnologies for the Life Sciences: Wiley-VCH Verlag GmbH & Co. KGaA 2007.
[9] Houska CR, Warren BE. X-Ray Study of the Graphitization of Carbon Black. Journal of Applied Physics. 1954;25(12):1503-9.
[10] Ungár T, Gubicza J, Tichy G, Pantea C, Zerda TW. Size and shape of crystallites and internal stresses in carbon blacks. Composites Part A: Applied Science and Manufacturing. 2005;36(4):431-6.
[11] Carmo M, Linardi M, Poco JGR. Characterization of nitric acid functionalized carbon black and its evaluation as electrocatalyst support for direct methanol fuel cell applications. Applied Catalysis A: General. 2009;355(1–2):132-8.
[12] Poh CK, Lim SH, Pan H, Lin J, Lee JY. Citric acid functionalized carbon materials for fuel cell applications. Journal of Power Sources. 2008;176(1):70-5.
[13] Rousseau S, Coutanceau C, Lamy C, Léger JM. Direct ethanol fuel cell (DEFC): Electrical performances and reaction products distribution under operating conditions with different platinum-based anodes. Journal of Power Sources. 2006;158(1):18-24.
[14] Leela Mohana Reddy A, Ramaprabhu S. Synthesis and Characterization of Magnetic Metal-encapsulated Multi-walled Carbon Nanobeads. Nanoscale Research Letters. 2008;3(2):76-81.
[15] Buchholz DB, Doherty SP, Chang RPH. Mechanism for the growth of multiwalled carbon-nanotubes from carbon black. Carbon. 2003;41(8):1625-34.
[16] Chen Z-G, Li F, Ren W-C, Hongtao C, Liu C, Lu GQ, et al. Double-walled carbon nanotubes synthesized using carbon black as the dot carbon source. Nanotechnology. 2006;17 13:3100-4.
[17] Doherty SP, Chang RPH. Synthesis of multiwalled carbon nanotubes from carbon black. Applied Physics Letters. 2002;81:2466 - 8.
[18] Bianco A, Kostarelos K, Prato M. Applications of carbon nanotubes in drug delivery. Current Opinion in Chemical Biology. 2005;9(6):674-9.
[19] Li D-C, Dai L, Huang S, Mau AWH, Wang ZL. Structure and growth of aligned carbon nanotube films by pyrolysis. Chemical Physics Letters. 2000;316(5–6):349-55.
[20] Ren Z, Lan Y, Wang Y. Introduction to Carbon. Aligned Carbon Nanotubes: Springer Berlin Heidelberg 2013, p. 1-5.

[21] Donnet JB, Bansal RC, Wang M-J. Carbon black - Science and technology: Marcel Dekker, New York; 1993.
[22] Lian W, Song H, Chen X, Li L, Huo J, Zhao M, et al. The transformation of acetylene black into onion-like hollow carbon nanoparticles at 1000°C using an iron catalyst. Carbon. 2008;46(3):525-30.
[23] Biscoe J, Warren BE. An X-Ray Study of Carbon Black. Journal of Applied Physics. 1942;13(6):364-71.
[24] Bernal JD. The Structure of Graphite. Proceedings of the Royal Society of London Series A. 1924;106(740):749-73.
[25] Castro Neto AH, Guinea F, Peres NMR, Novoselov KS, Geim AK. The electronic properties of graphene. Reviews of Modern Physics. 2009;81(1):109.
[26] Iijima S. Helical microtubules of graphitic carbon. Nature. 1991;354(6348):56-8.
[27] Iijima S, Ichihashi T. Single-shell carbon nanotubes of 1-nm diameter. Nature. 1993;363(6430):603-5.
[28] Frank H, Candace C, Valerie M, Marco R, Mike OC. The element carbon. Carbon Nanotubes: CRC Press 2006, p. 1-18.
[29] Monthioux M, Serp P, Flahaut E, Razafinimanana M, Laurent C, Peigney A, et al. Introduction to Carbon Nanotubes. In: Bhushan B, ed. Springer Handbook of Nanotechnology: Springer Berlin Heidelberg 2010, p. 47-118.
[30] Bethune DS, Klang CH, de Vries MS, Gorman G, Savoy R, Vazquez J, et al. Cobalt-catalysed growth of carbon nanotubes with single-atomic-layer walls. Nature. 1993;363(6430):605-7.
[31] Ehlich R, Biro LP, Hertel IV. Growth of nanotubes by decomposition of C60 on transition metal surfaces. Synthetic Metals. 1999;103(1–3):2486-7.
[32] Kokai F, Nozaki I, Okada T, Koshio A, Kuzumaki T. Efficient growth of multi-walled carbon nanotubes by continuous-wave laser vaporization of graphite containing B4C. Carbon. 2011;49(4):1173-81.
[33] Li JL, Wang LJ, Bai GZ, Jiang W. Carbon tubes produced during high-energy ball milling process. Scripta Materialia. 2006;54(1):93-7.
[34] Mahanandia P, Vishwakarma PN, Nanda KK, Prasad V, Subramanyam SV, Dev SK, et al. Multiwall carbon nanotubes from pyrolysis of tetrahydrofuran. Materials Research Bulletin. 2006;41(12):2311-7.
[35] Martin BS, Kenneth BKT, Rodrigo GL, Milne WI, David BH, Meyyappan M. Carbon nanotubes by plasma-enhanced chemical vapor deposition. Pure Applied Chemistry. 2006;78(6):1117-25.
[36] Sen R, Suzuki S, Kataura H, Achiba Y. Growth of single-walled carbon nanotubes from the condensed phase. Chemical Physics Letters. 2001;349(5–6):383-8.
[37] Shaijumon MM, Ramaprabhu S. Synthesis of carbon nanotubes by pyrolysis of acetylene using alloy hydride materials as catalysts and their hydrogen adsorption studies. Chemical Physics Letters. 2003;374(5–6):513-20.
[38] Tang D, Sun L, Zhou J, Zhou W, Xie S. Two possible emission mechanisms involved in the arc discharge method of carbon nanotube preparation. Carbon. 2005;43(13):2812-6.
[39] Wang Y-H, Chiu S-C, Lin K-M, Li Y-Y. Formation of carbon nanotubes from polyvinyl alcohol using arc-discharge method. Carbon. 2004;42(12–13):2535-41.
[40] Wei S, Kang WP, Davidson JL, Huang JH. Aligned carbon nanotubes fabricated by thermal CVD at atmospheric pressure using Co as catalyst with NH3 as reactive gas. Diamond and Related Materials. 2006;15(11–12):1828-33.
[41] Wong TS, Wang CT, Chen KH, Chen LC, Ma KJ. Carbon nanotube growth by rapid thermal processing. Diamond and Related Materials. 2001;10(9–10):1810-3.

[42] Rodriguez NM. A review of catalytically grown carbon nanofibers. Journal of Materials Research. 1993;8:3233-50.
[43] Doherty SP, Chang RPH. Synthesis of multiwalled carbon nanotubes from carbon black. Applied Physics Letters. 2002;81:2466-8.
[44] Kishinevsky S, Nikitenko SI, Pickup DM, van-Eck ERH, Gedanken A. Catalytic Transformation of Carbon Black to Carbon Nanotubes. Chemistry of Materials. 2002;14(11):4498-501.
[45] Chen Z-G, Li F, Ren W-C, Cong H, Liu C, Lu GQ, et al. Double-walled carbon nanotubes synthesized using carbon black as the dot carbon source. Nanotechnology. 2006;17:3100-4.
[46] Donnet JB, Oulanti H, Le Huu T. Mechanism growth of multiwalled carbon nanotubes on carbon black. Diamond and Related Materials. 2008;17(7–10):1506-12.
[47] Leela Mohana Reddy A, Shaijumon MM, Ramaprabhu S. Alloy hydride catalyst route for the synthesis of single-walled carbon nanotubes, multi-walled carbon nanotubes and magnetic metal-filled multi-walled carbon nanotubes. Nanotechnology. 2006;17(21):5299-305.
[48] Franklin RE. Crystallite Growth in Graphitizing and Non-Graphitizing Carbons. Proceedings of the Royal Society of London Series A Mathematical and Physical Sciences. 1951;209(1097):196-218.
[49] Graham D, Kay WS. The morphology of thermally graphitized P-33 carbon black in relation to its adsorbent uniformity. Journal of Colloid Science. 1961;16(2):182-5.
[50] Fitzer E, Weisenburger S. Kinetics of graphitization within the first minute of heat treatment. Carbon. 1976;14(6):323-7.
[51] Hüttinger KJ, Rosenblatt U. Kinetics of the graphitization-induced dimensional changes of artificial carbons. Carbon. 1976;14(5):267-70.
[52] Yoo CS, Nellis WJ. Phase Transformations in Carbon Fullerenes at High Shock Pressures. Science. 1991;254(5037):1489-91.
[53] Butenko YV, Kuznetsov VL, Chuvilin AL, Kolomiichuk VN, Stankus SV, Khairulin RA, et al. Kinetics of the graphitization of dispersed diamonds at “low” temperatures. Journal of Applied Physics. 2000;88(7):4380-8.
[54] Wang X, Zhang GM, Zhang YL, Li FY, Yu RC, Jin CQ, et al. Graphitization of glassy carbon prepared under high temperatures and high pressures. Carbon. 2003;41(1):188-91.
[55] Harris PJF. New Perspectives on the Structure of Graphitic Carbons. Critical Reviews in Solid State and Materials Sciences. 2005;30(4):235-53.
[56] McEnaney B. Adsorption and structure in microporous carbons. Carbon. 1988;26(3):267-74.
[57] Harris PJF. Structure of non-graphitising carbons. International Materials Reviews. 1997;42(5):206-18.
[58] Foley HC. Carbogenic molecular sieves: synthesis, properties and applications. Microporous Materials. 1995;4(6):407-33.
[59] Zhili Z, Brydson R, Reddy S, Westwood A, Brown A, Rand B. Nanostructural development of non-graphitising carbons probed using TEM/EELS: The importance of fullerenes? Journal of Physics: Conference Series. 2010;241(1):012094.
[60] Marsh PA, Voet A, Mullens TJ, Price LD. Quantitative micrography of carbon black microstructure. Carbon. 1971;9(6):797-805.
[61] Cataldo F. The impact of a fullerene-like concept in carbon black science. Carbon. 2002;40(2):157-62.

[62] Johnson MP, Locke RW, Donnet JB, Wang TK, Wang CC, Bertrand P. Carbon Black and Fullerenes: New Discoveries in Early Formation Mechanisms and Nucleation. Rubber Chemistry and Technology. 2000;73(5):875-88.
[63] Zhang QL, O'Brien SC, Heath JR, Liu Y, Curl RF, Kroto HW, et al. Reactivity of large carbon clusters: spheroidal carbon shells and their possible relevance to the formation and morphology of soot. The Journal of Physical Chemistry. 1986;90(4):525-8.
[64] Kroto HW, McKay K. The formation of quasi-icosahedral spiral shell carbon particles. Nature. 1988;331:328-31.
[65] Vander Wal RL, Tomasek AJ, Street K, Hull DR, Thompson WK. Carbon Nanostructure Examined by Lattice Fringe Analysis of High-Resolution Transmission Electron Microscopy Images. Appl Spectrosc. 2004;58(2):230-7.
[66] Setlur AA, Doherthy SP, Dai JY, Chang RPH. A promising pathway to make multiwalled carbon nanotubes Appl Phys Lett. 2000;76.
[67] Doherty SP, Chang RPH. Synthesis of multiwalled carbon nanotubes from carbon black. Appl Phys Lett. 2002;81.
[68] Doherty SP, Buchholz DB, Chang RPH. Semi-continous production of multiwalled carbon nanotubes using magnetic field assisted arc furnace. Carbon. 2006;44.
[69] Lian W, Song H, Chen X, Li L, Huo J, Zhao M, et al. The transformation of acetylene black into onion-like hollow carbon nanoparticles at 1000 °C using an iron catalyst. Carbon. 2008;46(3):525-30.
[70] Chahan Y, Klavs H, Francois D, Robert L W. Coalescence reactions of fullerenes. Nature. 1992;359:44-7.
[71] Shen W, Huggins FE, Shah N, Jacobs G, Wang Y, Shi X, et al. Novel Fe–Ni nanoparticle catalyst for the production of CO- and CO2-free H2 and carbon nanotubes by dehydrogenation of methane. Applied Catalysis A: General. 2008;351(1):102-10.
[72] Cheng J, Zou XP, Zhu G, Wang MF, Su Y, Yang GQ, et al. Synthesis of iron-filled carbon nanotubes with a great excess of ferrocene and their magnetic properties. Solid State Communications. 2009;149(39–40):1619-22.
[73] Cacciamani G, Dinsdale A, Palumbo M, Pasturel A. The Fe–Ni system: Thermodynamic modelling assisted by atomistic calculations. Intermetallics. 2010;18(6):1148-62.
[74] Zhang C, Li J, Shi C, Liu E, Du X, Feng W, et al. The efficient synthesis of carbon nano-onions using chemical vapor deposition on an unsupported Ni–Fe alloy catalyst. Carbon. 2011;49(4):1151-8.
[75] Bhaviripudi S, Mile E, Steiner SA, Zare AT, Dresselhaus MS, Belcher AM, et al. CVD Synthesis of Single-Walled Carbon Nanotubes from Gold Nanoparticle Catalysts. Journal of the American Chemical Society. 2007;129(6):1516-7.
[76] Shen W, Huggins FE, Shah N, Jacobs G, Wang Y, Shi X, et al. Novel Fe-Ni nanoparticle catalyst for the production of CO- and CO2-free H2 and carbon nanotubes by dehydrogenation of methane. Applied Catalysis A: General. 2008;351(1):102-10.
[77] Luo G, Li Z, Wei F, Xiang L, Deng X, Jin Y. Catalysts effect on morphology of carbon nanotubes prepared by catalytic chemical vapor deposition in a nano-agglomerate bed. Physica B: Condensed Matter. 2002;323(1-4):314-7.
[78] Lv R, Kang F, Cai D, Wang C, Gu J, Wang K, et al. Long continuous FeNi nanowires inside carbon nanotubes: Synthesis, property and application. Journal of Physics and Chemistry of Solids. 2008;69(5–6):1213-7.
[79] Sengupta J, Jacob C. The effect of Fe and Ni catalysts on the growth of multiwalled carbon nanotubes using chemical vapor deposition. Journal of Nanoparticle Research. 2010;12(2):457-65.

[80] Wu H, Qian C, Cao Y, Cao P, Li W, Zhang X, et al. Synthesis and magnetic properties of size-controlled FeNi alloy nanoparticles attached on multiwalled carbon nanotubes. Journal of Physics and Chemistry of Solids. 2010;71(3):290-5.
[81] Chiang W-H, Sankaran RM. The influence of bimetallic catalyst composition on single-walled carbon nanotube yield. Carbon. 2012;50(3):1044-50.
[82] Tsoufis T, Xidas P, Jankovic L, Gournis D, Saranti A, Bakas T, et al. Catalytic production of carbon nanotubes over Fe-Ni bimetallic catalysts supported on MgO. Diamond and Related Materials. 2007;16(1):155-60.
[83] Qian W, Liu T, Wang Z, Yu H, Li Z, Wei F, et al. Effect of adding nickel to iron-alumina catalysts on the morphology of as-grown carbon nanotubes. Carbon. 2003;41(13):2487-93.
[84] Zhou W, Han Z, Wang J, Zhang Y, Jin Z, Sun X, et al. Copper Catalyzing Growth of Single-Walled Carbon Nanotubes on Substrates. Nano Letters. 2006;6(12):2987-90.
[85] Yuan D, Ding L, Chu H, Feng Y, McNicholas TP, Liu J. Horizontally Aligned Single-Walled Carbon Nanotube on Quartz from a Large Variety of Metal Catalysts. Nano Letters. 2008;8(8):2576-9.
[86] Watson EB. Diffusion and solubility of C in Pt. Journal Name: Am Mineral; (United States); Journal Volume: 72:5-6.Medium: X; Size: Pages: 487-90.
[87] Heckman FA, Harling DF. Progressive Oxidation of Selected Particles of Carbon Black: Further Evidence for a New Microstructural Model. Rubber Chemistry and Technology. 1966;39(1):1-13.
[88] Thomas WJ. Effect of oxidation on the pore structure of some graphitized carbon blacks. Carbon. 1966;3(4):435-43.
[89] Voet A, Donnet JB, Marsh PA, Schultz J. Spontaneous generation of large laminae in oxidized carbon blacks. Carbon. 1966;4(2):155-7.
[90] Kamegawa K, Nishikubo K, Yoshida H. Oxidative degradation of carbon blacks with nitric acid (I)—Changes in pore and crystallographic structures. Carbon. 1998;36(4):433-41.
[91] Neeft JPA, Makkee M, Moulijn JA. Catalytic oxidation of carbon black — I. Activity of catalysts and classification of oxidation profiles. Fuel. 1998;77(3):111-9.
[92] Kamegawa K, Nishikubo K, Kodama M, Adachi Y, Yoshida H. Oxidative degradation of carbon blacks with nitric acid: II. Formation of water-soluble polynuclear aromatic compounds. Carbon. 2002;40(9):1447-55.
[93] Smith RC, Tomarelli RC, Howard HC. Oxidation of Carbonaceous Materials to Organic Acids by Oxygen at Elevated Pressures. Journal of the American Chemical Society. 1939;61(9):2398-402.
[94] Pradhan BK, Sandle NK. Effect of different oxidizing agent treatments on the surface properties of activated carbons. Carbon. 1999;37(8):1323-32.
[95] Carmo M, Linardi M, Rocha Poco JG. H2O2 treated carbon black as electrocatalyst support for polymer electrolyte membrane fuel cell applications. International Journal of Hydrogen Energy. 2008;33(21):6289-97.
[96] Borah D, Satokawa S, Kato S, Kojima T. Characterization of chemically modified carbon black for sorption application. Applied Surface Science. 2008;254(10):3049-56.
[97] Carmo M, Brandalise M, Neto AO, Spinacé EV, Taylor AD, Linardi M, et al. Enhanced activity observed for sulfuric acid and chlorosulfuric acid functionalized carbon black as PtRu and PtSn electrocatalyst support for DMFC and DEFC applications. International Journal of Hydrogen Energy. 2011;36(22):14659-67.
[98] Hiura H, Ebbesen TW, Tanigaki K. Opening and purification of carbon nanotubes in high yields. Advanced Materials. 1995;7(3):275-6.

[99] Mul G, Neeft JPA, Kapteijn F, Moulijn JA. The formation of carbon surface oxygen complexes by oxygen and ozone. The effect of transition metal oxides. Carbon. 1998;36(9):1269-76.
[100] Oshikiri M, Yokono T, Sanada Y. Surface characterization of carbon black modified by oxygen plasma. J Mater Sci Lett. 1989;8(11):1269-70.
[101] Takada T, Nakahara M, Kumagai H, Sanada Y. Surface modification and characterization of carbon black with oxygen plasma. Carbon. 1996;34(9):1087-91.
[102] Bergemann K, Fanghänel E, Knackfuß B, Lüthge T, Schukat G. Modification of carbon black properties by reaction with maleic acid derivatives. Carbon. 2004;42(11):2338-40.
[103] Zhou X, Li Q, Wu C. Grafting of maleic anhydride onto carbon black surface via ultrasonic irradiation. Applied Organometallic Chemistry. 2008;22(2):78-81.
[104] Dresselhaus MS, Dresselhaus G, Saito R, Jorio A. Raman spectroscopy of carbon nanotubes. Physics Reports. 2005;409(2):47-99.
[105] Chu PK, Li L. Characterization of amorphous and nanocrystalline carbon films. Materials Chemistry and Physics. 2006;96(2–3):253-77.
[106] Ferrari AC. Raman spectroscopy of graphene and graphite: Disorder, electron–phonon coupling, doping and nonadiabatic effects. Solid State Communications. 2007;143(1–2):47-57.
[107] Ferrari AC, Robertson J. Raman spectroscopy of amorphous, nanostructured, diamond–like carbon, and nanodiamond. Phil Trans R Soc A. 2004;362(1824):2477-512.
[108] Jawhari T, Roid A, Casado J. Raman spectroscopic characterization of some commercially available carbon black materials. Carbon. 1995;33(11):1561-5.
[109] Lespade P, Al-Jishi R, Dresselhaus MS. Model for Raman scattering from incompletely graphitized carbons. Carbon. 1982;20(5):427-31.
[110] Malard LM, Pimenta MA, Dresselhaus G, Dresselhaus MS. Raman spectroscopy in graphene. Physics Reports. 2009;473(5–6):51-87.
[111] Nakamizo M. Raman spectra of iron-containing glassy carbons. Carbon. 1991;29(6):757-61.
[112] Nakamizo M, Kammereck R, Walker Jr PL. Laser raman studies on carbons. Carbon. 1974;12(3):259-67.
[113] Reich S, Thomsen C. Raman spectroscopy of graphite. Phil Trans R Soc A. 2004;362:2271-88.
[114] Tuinstra F, Koenig JL. Raman spectrum of graphite. J Chem Phys. 1970;53:1126-30.
[115] Ferrari AC, Robertson J. Interpretation of Raman spectra of disordered and amorphous carbon. Phys Rev B. 2000;61(20):14095-107.
[116] Lehman JH, Terrones M, Mansfield E, Hurst KE, Meunier V. Evaluating the characteristics of multiwall carbon nanotubes. Carbon. 2011;49(8):2581-602.
[117] Robertson J. Properties of diamond-like carbon. Surface and Coatings Technology. 1992;50(3):185-203.
[118] Pimenta MA, Dresselhaus G, Dresselhaus MS, Cancado LG, Jorio A, Saito R. Studying disorder in graphite-based systems by Raman spectroscopy. Physical Chemistry Chemical Physics. 2007;9(11):1276-90.
[119] van Zuilen MA, Fliegel D, Wirth R, Lepland A, Qu Y, Schreiber A, et al. Mineral-templated growth of natural graphite films. Geochimica et Cosmochimica Acta. 2012;83(0):252-62.
[120] Williams D, Carter CB. The Transmission Electron Microscope. Transmission Electron Microscopy: Springer US 2009, p. 3-22.
[121] Jäger C, Henning T, Schlögl R, Spillecke O. Spectral properties of carbon black. Journal of Non-Crystalline Solids. 1999;258(1–3):161-79.

[122] Endo M. Carbon Nanotubes Research: Past and Future. Jpn J Appl Phys. 2012;51:040001-9.
[123] Endo M, Takeuchi K, Hiraoka T, Furuta T, Kasai T, Sun X, et al. Stacking nature of graphene layers in carbon nanotubes and nanofibres. Journal of Physics and Chemistry of Solids. 1997;58(11):1707-12.
[124] Committee ASMIH. ASM Handbook, Volume 10 - Materials Characterization. ASM International.
[125] Warren BE. X-Ray Diffraction Study of Carbon Black. The Journal of Chemical Physics. 1934;2(9):551-5.
[126] Warren BE. X-Ray Diffraction in Random Layer Lattices. Phys Rev. 1941;59(9):693-8.
[127] Alexander L, Darin SR. Erratum : X-Ray Diffraction Study of Four Reinforcing Carbon Blacks. The Journal of Chemical Physics. 1956;24(5):1118-.
[128] Alexander LE, Sommer EC. Systematic Analysis of Carbon Black Structures. The Journal of Physical Chemistry. 1956;60(12):1646-9.
[129] Fuente E, Menéndez JA, Díez MA, Suárez D, Montes-Morán MA. Infrared Spectroscopy of Carbon Materials: A Quantum Chemical Study of Model Compounds. The Journal of Physical Chemistry B. 2003;107(26):6350-9.
[130] Brunauer S, Emmett PH, Teller E. Adsorption of Gases in Multimolecular Layers. Journal of the American Chemical Society. 1938;60(2):309-19.
[131] Asokan V, Velauthapillai D, Løvlie R, Madsen D. Effect of substrate and catalyst on the transformation of carbon black into nanotubes. J Mater Sci: Mater Electron. 2013;24(9):3231-9.
[132] Kukovitsky EF, L'Vov SG, Sainov NA, Shustov VA, Chernozatonskii LA. Correlation between metal catalyst particle size and carbon nanotube growth. Chemical Physics Letters. 2002;355(5–6):497-503.
[133] Ward JW, Wei BQ, Ajayan PM. Substrate effects on the growth of carbon nanotubes by thermal decomposition of methane. Chemical Physics Letters. 2003;376(5–6):717-25.
[134] lijima S, Ichihashi T, Ando Y. Pentagons, heptagons and negative curvature in graphite microtubule growth. Nature. 1992;356:776-8.
[135] Brabec CJ, Maiti A, Bernholc J. Structural defects and the shape of large fullerenes. Chemical Physics Letters. 1994;219(5–6):473-8.
[136] Asokan V, Madsen D, Velaug M, Kosinski P. Effect of Temperature on the Transformation of Carbon Black into Nanotubes. Advanced Materials Research. 2014;875 - 877:1565-71.
[137] Iwashita N, Park CR, Fujimoto H, Shiraishi M, Inagaki M. Specification for a standard procedure of X-ray diffraction measurements on carbon materials. Carbon. 2004;42(4):701-14.
[138] Harris PJF. Carbon Nanotube Science: Cambridge University Press 2009.
[139] Asokan V, Madsen DN, Kosinski P, Myrseth V. Transformation of carbon black into carbon nano-beads and nanotubes: The effect of catalysts. New Carbon Materials. 2015;30(1):19-29.
[140] Rodriguez NM, Kim MS, Fortin F, Mochida I, Baker RTK. Carbon deposition on iron-nickel alloy particles. Applied Catalysis A: General. 1997;148(2):265-82.
[141] Lu Y, Zhu Z, Liu Z. Catalytic growth of carbon nanotubes through CHNO explosive detonation. Carbon. 2004;42(2):361-70.
[142] Kumar M, Ando Y. Chemical Vapor Deposition of Carbon Nanotubes: A Review on Growth Mechanism and Mass Production. Journal of Nanoscience and Nanotechnology. 2010;10:3739–58.

[143] Jourdain V, Bichara C. Current understanding of the growth of carbon nanotubes in catalytic chemical vapour deposition. Carbon. 2013;58(0):2-39.
[144] Amelinckx S, Zhang XB, Bernaerts D, Zhang XF, Ivanov V, Nagy JB. A Formation Mechanism for Catalytically Grown Helix-Shaped Graphite Nanotubes. Science. 1994;265(5172):635-9.
[145] Kang JL, Li JJ, Du XW, Shi CS, Zhao NQ, Cui L, et al. Synthesis and growth mechanism of metal filled carbon nanostructures by CVD using Ni/Y catalyst supported on copper. Journal of Alloys and Compounds. 2008;456(1–2):290-6.
[146] Cheng J, Zou X-p, Li F, Zhang H-d, Ren P-f. Synthesis of bamboo-like carbon nanotubes by ethanol catalytic combustion technique. Transactions of Nonferrous Metals Society of China. 2006;16, Supplement 1(0):s435-s7.
[147] González I, De Jesus J, Cañizales E. Bamboo-shaped carbon nanotubes generated by methane thermal decomposition using Ni nanoparticles synthesized in water–oil emulsions. Micron. 2011;42(8):819-25.
[148] Charlier JC, Amara H, Lambin P. Catalytically Assisted Tip Growth Mechanism for Single-Wall Carbon Nanotubes. ACS Nano. 2007;1(3):202-7.
[149] Popov VN. Carbon nanotubes: properties and application. Materials Science and Engineering: R: Reports. 2004;43(3):61-102.
[150] Liu B, Jia D, Meng Q, Rao J. A novel method for preparation of hollow carbon spheres under a gas pressure atmosphere. Carbon. 2007;45(3):668-70.
[151] Parmon VN. Fluidization of the active component of catalysts in catalytic formation of carbon assisted by iron and nickel carbides. Catalysis Letters. 1996;42(3):195-9.
[152] Asokan V, Myrseth V, Kosinski P. Effect of Pt and Fe catalysts in the transformation of carbon black into carbon nanotubes. Journal of Physics and Chemistry of Solids. 2015;81(0):106-15.
[153] Rao CNR, Govindaraj A. Carbon Nanotubes from Organometallic Precursors. Accounts of Chemical Research. 2002;35(12):998-1007.
[154] Rao CNR, Kulkarni GU, Govindaraj A, Satishkumar BC, John Thomas P. Metal nanoparticles, nanowires, and carbon nanotubes. Pure and Applied Chemistry. 2000;72(1–2):21–33.
[155] Rao CNR, Sen R. Large aligned-nanotube bundles from ferrocene pyrolysis. Chemical Communications. 1998(15):1525-6.
[156] Nadagouda MN, Varma RS. Green and controlled synthesis of gold and platinum nanomaterials using vitamin B2: density-assisted self-assembly of nanospheres, wires and rods. Green Chemistry. 2006;8(6):516-8.
[157] Qiu H, Yang G, Zhao B, Yang J. Catalyst-free synthesis of multi-walled carbon nanotubes from carbon spheres and its implications for the formation mechanism. Carbon. 2013;53(0):137-44.
[158] Du G, Song C, Zhao J, Feng S, Zhu Z. Solid-phase transformation of glass-like carbon nanoparticles into nanotubes and the related mechanism. Carbon. 2008;46(1):92-8.
[159] Smith BW, Monthioux M, Luzzi DE. Encapsulated C60 in carbon nanotubes. Nature. 1998;396:323-4.
[160] Smith BW, Luzzi DE. Formation mechanism of fullerene peapods and coaxial tubes: a path to large scale synthesis. Chemical Physics Letters. 2000;321(1–2):169-74.
[161] Hernández E, Meunier V, Smith BW, Rurali R, Terrones H, Buongiorno Nardelli M, et al. Fullerene Coalescence in Nanopeapods: A Path to Novel Tubular Carbon. Nano Letters. 2003;3(8):1037-42.
[162] Yahachi S, Keishi N, Kenichiro K, Takehisa M. Carbon nanocapsules and single-layered nanotubes produced with platinum-group metals (Ru, Rh, Pd, Os, Ir, Pt) by arc discharge. Journal of Applied Physics. 1996;80(5):3062-7.

[163] Height MJ, Howard JB, Tester JW, Vander Sande JB. Carbon Nanotube Formation and Growth via Particle−Particle Interaction. The Journal of Physical Chemistry B. 2005;109(25):12337-46.
[164] Du G, Feng S, Zhao J, Song C, Bai S, Zhu Z. Particle−Wire−Tube Mechanism for Carbon Nanotube Evolution. Journal of the American Chemical Society. 2006;128(48):15405-14.
[165] Ding F, Larsson P, Larsson JA, Ahuja R, Duan H, Rosén A, et al. The Importance of Strong Carbon−Metal Adhesion for Catalytic Nucleation of Single-Walled Carbon Nanotubes. Nano Letters. 2007;8(2):463-8.
[166] Al-Hartomy OA, Al-Solamy F, Al-Ghamdi A, Dishovsky N, Ivanov M, Mihaylov M, et al. Influence of Carbon Black Structure and Specific Surface Area on the Mechanical and Dielectric Properties of Filled Rubber Composites. International Journal of Polymer Science. 2011;2011:1-8.
[167] Asokan V, Kosinski P, Skodvin T, Myrseth V. Characterization of carbon black modified by maleic acid. Front Mater Sci. 2013;7(3):302-7.
[168] Donnet JB. The chemical reactivity of carbons. Carbon. 1968;6(2):161-76.
[169] Donnet JB. Structure and reactivity of carbons: From carbon black to carbon composites. Carbon. 1982;20(4):267-82.
[170] Liu Y-q, Chen X-h, Yang Z, Pu Y-x, Yi B. Synthesis of aligned carbon nanotube with straight-chained alkanes by nebulization method. Transactions of Nonferrous Metals Society of China. 2010;20(6):1012-6.
[171] Montoro LA, Corio P, Rosolen JM. A comparative study of alcohols and ketones as carbon precursor for multi-walled carbon nanotube growth. Carbon. 2007;45(6):1234-41.
[172] Esconjauregui S, Whelan CM, Maex K. The reasons why metals catalyze the nucleation and growth of carbon nanotubes and other carbon nanomorphologies. Carbon. 2009;47(3):659-69.
[173] Wirth CT, Hofmann S, Robertson J. State of the catalyst during carbon nanotube growth. Diamond and Related Materials. 2009;18(5–8):940-5.
[174] Stauf GT, Driscoll DC, Dowben PA, Barfuss S, Grade M. Iron and nickel thin film deposition via metallocene decomposition. Thin Solid Films. 1987;153(1–3):421-30.
[175] Song H, Chen X. Large-scale synthesis of carbon-encapsulated iron carbide nanoparticles by co-carbonization of durene with ferrocene. Chemical Physics Letters. 2003;374(3–4):400-4.
[176] Maruyama S, Kojima R, Miyauchi Y, Chiashi S, Kohno M. Low-temperature synthesis of high-purity single-walled carbon nanotubes from alcohol. Chemical Physics Letters. 2002;360(3–4):229-34.
[177] Roy D, Chhowalla M, Wang H, Sano N, Alexandrou I, Clyne TW, et al. Characterisation of carbon nano-onions using Raman spectroscopy. Chemical Physics Letters. 2003;373(1–2):52-6.
[178] Liao X-H, Zhu J-J, Chen H-Y. Microwave synthesis of nanocrystalline metal sulfides in formaldehyde solution. Materials Science and Engineering: B. 2001;85(1):85-9.
[179] Phoempoon P, Sikong L. Phase Transformation of VO2 Nanoparticles Assisted by Microwave Heating. The Scientific World Journal. 2014;2014:8.
[180] Chen D, Tang K, Shen G, Sheng J, Fang Z, Liu X, et al. Microwave-assisted synthesis of metal sulfides in ethylene glycol. Materials Chemistry and Physics. 2003;82(1):206-9.
[181] Apte SK, Naik SD, Sonawane RS, Kale BB, Pavaskar N, Mandale AB, et al. Nanosize Mn3O4 (Hausmannite) by microwave irradiation method. Materials Research Bulletin. 2006;41(3):647-54.

[182] Rao KJ, Ramesh PD. Use of microwaves for the synthesis and processing of materials. Bull Mater Sci. 1995;18(4):447-65.
[183] Park S-J, Kim J-S. Role of Chemically Modified Carbon Black Surfaces in Enhancing Interfacial Adhesion between Carbon Black and Rubber in a Composite System. Journal of Colloid and Interface Science. 2000;232(2):311-6.
[184] Grundke K, Boerner M, Jacobasch HJ. Characterization of fillers and fibres by wetting and electrokinetic measurements. Colloids and Surfaces. 1991;58(1–2):47-59.
[185] Burg P, Cagniant D. Characterization of Carbon Surface Chemistry. Chemistry & Physics of Carbon: CRC Press 2007, p. 129-75.